INTERACTION OF SEA WAVES WITH DISCRETE ICE FLOES

by

Nobuhisa Kobayashi
and
David G. Cannon

Sponsored by

U. S. Army Cold Regions Research and Engineering Laboratory

Research Report No. CE-87-64

Ocean Engineering Program
Department of Civil Engineering
University of Delaware
Newark, Delaware
August, 1987

ABSTRACT

A quantitative understanding of wave and ice interaction is essential for designing structures in partially ice-covered waters. At present, the ice is modelled either as a thin elastic or inelastic plate or as a rigid body, depending on the length and time scales involved in a specific problem, while potential flow theory is normally used assuming that the water is incompressible and inviscid and the flow is irrotational.

First, the flexural response of elastic ice floes under the action of normally-incident regular waves in finite water depth is analyzed assuming that a row of the ice flows may be regarded as a long thin elastic raft of finite width. The analysis relates the flexural displacement of the elastic raft to the wave reflection and transmission through the raft. Moreover, the mean wave drift force on the two-dimensional raft is expressed in terms of the wave reflection and transmission coefficients. The general solution derived for finite water depth is then approximated for deep water depth to reduce the required computational efforts considerably. The computational procedure for the approximate deep-water solution, which is explained in detail, is to compute the wave reflection and transmission coefficients, the flexural displacement of the ice and the wave drift force on the ice.

Second, the motion of a rigid ice floe of finite thickness under the action of incident regular waves is analyzed assuming that the ice floe is vertically axisymmetric. The analysis accounts for the waves scattered and radiated by the oscillating ice floe. Considering momentum balance, the wave drift force acting on the three-dimensional rigid body is expressed in terms

of the scattered and radiated waves in the far field. The accuracy and limitation of the boundary integral equation method used in the report is discussed by comparing the numerical method with available analytical and numerical solutions as well as with small-scale model tests.

Third, the computed results for elastic and rigid ice floes are presented to elucidate the wave and ice interaction and examine the similarity and differences between elastic and rigid ice floes. The computed results indicate that the effects of sea waves on an ice floe depend on the size of the ice floe relative to the incident wavelength. Furthermore, the wave drift force will be important in the force balance associated with the horizontal movement of an elastic or rigid ice floe if the surface waves in partially ice-covered water are not negligible.

ACKNOWLEDGEMENTS

This study was sponsored by the U. S. Army Cold Regions Research and Engineering Laboratory under Contract No. DACA 89-86-K-0005. The authors would like to express their gratitude for the financial support.

TABLE OF CONTENTS

LIST OF FIGURES

1.0 INTRODUCTION

1.1 Background

Structures in partially ice-covered waters such as the Bering Sea and the Great Lakes must be designed so as to withstand design ice and wave forces which will probably occur separately. In addition, these structures must be designed against the impact force associated with ice floes floating in waves and colliding against structures since large waves generated in the open water break and penetrate the ice cover well inside the ice edge (Wadhams, 1986). Consequently, quantitative knowledge of wave propagation in the field of discrete floes and resulting motion of ice floes is essential for predicting the effects of wave and ice interaction on the structures.

Furthermore, wind-generated waves exert mean drift forces on ice floes and affect the large-scale horizontal movement of ice floes which may be caused by winds and currents. As a result, the mean wave drift force should be included in the ice floe force balance used for predicting the horizontal movement of ice floes in partially ice-covered waters (Madsen et al., 1986).

In the following, previous studies on the wave and ice interaction are briefly reviewed to elucidate the present knowledge of this subject. At present, the ice is modelled either as a thin elastic or inelastic plate or as a rigid body, while the wave motion is analyzed using linear potential flow theory assuming that the water is incompressive and inviscid and the small-amplitude wave motion is irrotational.

1.2 Previous Studies

The interaction of waves with the ice cover determines the size

distribution of ice floes broken by wave action and the wave conditions affected by the ice cover. Kheisin (1967) summarized the mathematical models concerning wave propagation through floating thin elastic ice sheets as well as in the ice field of pancake type which was treated as a continuous cover of small non-interacting mass points. In order to describe the slow attenuation of ocean waves as they penetrate the ice sheet, Wadhams (1973) and Squire (1984b) accounted for inelastic flexure of the ice sheet. Squire (1984a) analyzed the refraction of obliquely incident waves at the edge of the thin elastic ice sheet and proposed a breakup mechanism based on the modulation of wave amplitude with distance from the edge. The wave-induced flexure of an ice floe or island may cause the fracture and breakup of the ice mass (Squire, 1983a; Goodman et al., 1980). On the other hand, the attenuation of wave energy in the field of discrete floes was investigated by assuming a row of ice floes to be an infinitely long elastic raft of finite width and analyzing the reflection and transmission of normally incident waves through a series of rows of ice floes (Wadhams, 1986). Field measurements of the wave and ice interaction in the vicinity of ice edges were also conducted to calibrate and verify these theories (Squire, 1983b; Wadhams et al., 1985). Although significant progress has been made, more extensive verification of these theories will be required to apply them to practical engineering problems. Furthermore, the interaction of waves with the ice cover may also be important in nearshore regions. Mollo-Christensen (1983a) investigated the interaction of edge waves with the shore fast ice sheet as a possible cause of ice rideup on beaches. Andersen et al. (1984) conducted field and tank tests to examine a possible utilization of artificially-generated waves to break and transport the ice formed in a harbor.

For given wave and ice conditions at a specific location, the motion of an ice floe may be predicted by assuming the floe to be a rigid body rather than a thin elastic plate since the analysis based on the plate approximation accounts for the vertical displacement of the plate only. The motion of a rigid ice floe due to waves may be separated into the six oscillatory modes corresponding to surge, sway, heave, roll, pitch and yaw and the wave-induced drift (Mei, 1983; Sarpkaya et al., 1981). The wave-induced drift is caused by the mean wave force which is normally neglected for predicting the horizontal movement of an ice floe or iceberg due to wind, currents, Coriolis force and a mean sea surface tilt (Madsen et al., 1986; Sodhi et al., 1980). The two-dimensional wave drift experiments conducted by Harms (1986) suggested a floe with 10 m width could attain speeds as high as 1 m/sec for steep ocean waves. Furthermore, Wadhams (1983) showed that the wave drift force acting on a floe of 20 m diameter could be larger than the corresponding wind drag force although the drift force was estimated using the theory of Longuet-Higgins (1977) for a two-dimensional body in normally incident waves. In addition to the wave drift force, the oscillatory component of the relative velocity of the water with respect to a floe will modify the hydrodynamic drag force acting on the floe due to currents (Mollo-Christensen, 1983b).

The impact load resulting from a moving iceberg colliding against an offshore structure is a concern to exploration operations and production systems off the east coast of Canada. Lever et al. (1984) conducted small-scale model tests on the wave-induced motion of small icebergs and bergy bits and concluded that these ice masses in storm waves could attain very large kinetic energies. Johnson et al. (1985) used a simple energy-based model which assumes that the work done by crushing ice equals the iceberg kinetic

energy immediately before the impact. Thus, the kinetic energy of an ice mass is closely related to its impact load on an offshore structure. On the other hand, Salvalaggio et al. (1986) employed a momentum-based model to simulate more detailed impact dynamics numerically. In any case, these models require the iceberg velocity immediately before the impact as input. Isaacson et al. (1986) developed a numerical model for predicting the motions of an ice mass prior to impact with a large fixed offshore structure. The model consists of a two-body diffraction solution for wave-induced oscillations and a time-stepping procedure for drift motions. The computed results for several examples indicated that the velocity and added mass of the ice mass and its trajectory prior to impact might be significantly altered from their far-field values because of the hydrodynamic interactions arising from the increasingly close proximity of the ice mass and structure. At present, available models related to ice impact loads are limited to a single ice mass impacting a large gravity based structure.

1.3 Report Organization

In Section 2.0, the flexural response of elastic ice floes under the action of normally-incident regular waves in finite water depth is analyzed assuming a row of the ice floes may be regarded as a long thin elastic raft of finite width. The present analysis improves the approximate solution for deep water depth presented by Wadhams (1983, 1986) since the approximate solution does not satisfy the required matching conditions at the edges of the raft. The analysis shows that the flexural response of the elastic raft is directly related to the wave reflection and transmission through the raft. The wave drift force on the two-dimensional raft also depends on the wave reflection and transmission coefficients. In order to simplify the required

computational procedure significantly, the general solution derived for finite water depth is approximated for deep water depth. The computational procedure for the approximate deep-water solution is then explained in detail.

In Section 3.0, an analysis is performed of the response of a rigid ice floe of finite thickness under the action of incident linear waves. The floe is assumed to be vertically axisymmetric to reduce the required computational effort. The analysis considers the linear waves scattered and radiated by the rigid ice floe which oscillates horizontally and vertically as well as rotates about the horizontal axis perpendicular to the direction of incident wave propagation. Furthermore, the wave drift force acting on the three-dimensional rigid body is expressed in terms of the scattered and radiated waves in the far field by considering momentum balance. The numerical method based on the boundary integral equations adopted in the report is then compared with available analytical and numerical solutions as well as with small-scale model tests in order to examine the accuracy and limitation of the adopted method.

In Section 4.0, the computed results for elastic and rigid ice floes are presented to gain a physical insight into the mechanism of the wave and ice interaction. Comparison is also made of the computed results for the elastic and rigid ice floes to examine the sensitivity of the computed results to the basic assumptions regarding the ice characteristics and response.

In Section 5.0, the summary and conclusions of this study are presented. Limitations and future improvements of the analyses and computations presented in this report are explained in light of the complicated ice and wave interactions which occur in actual field conditions.

The references quoted in the report are listed alphabetically in Appendix I. The symbols used in the report are listed in Appendix II.

2.0 ELASTIC ICE FLOES

In this section, an ice floe is assumed to be a thin elastic plate of horizontal length D and uniform thickness h. Furthermore, a row of the ice floes is assumed to form and be regarded as a long elastic raft of width D perpendicular to incident monochromatic waves, which are assumed to be described by linear (small-amplitude) wave theory. The use of linear wave theory will be appropriate if the incident wave height, H, is small relative to the wavelength, L, and the water depth, d, which is assumed to be constant. The quantities of interest in the following analysis are the flexural oscillation of the elastic raft, the wave reflection and transmission coefficients and the mean wave drift force acting on the raft.

2.1 Wave Reflection and Transmission

The two-dimensional problem analyzed here is illustrated in Fig. 1 where the Cartesian coordinate system (x,z) used in the following analysis is defined. The x-axis is taken to be positive in the direction of incident wave propagation, whereas the z-axis is positive vertically upwards from the still water level (SWL). The elastic raft of width D and thickness h is assumed to be floating freely. Consequently, the depth of submergence below SWL, h_s, in the absence of the wave action is given by $h_s = (\rho_i/\rho)h$ in which ρ = density of the water and ρ_i = density of the ice. Since $\rho > \rho_i$, hence $h_s<h$. The thickness h of the ice is assumed to be small relative to the width D, the incident wavelength L, and the water depth d. The normally-incident linear wave causes the flexural motion of the thin ice raft, while the presence of the raft produces the reflected and transmitted waves propagating in the negative and positive x-direction, respectively.

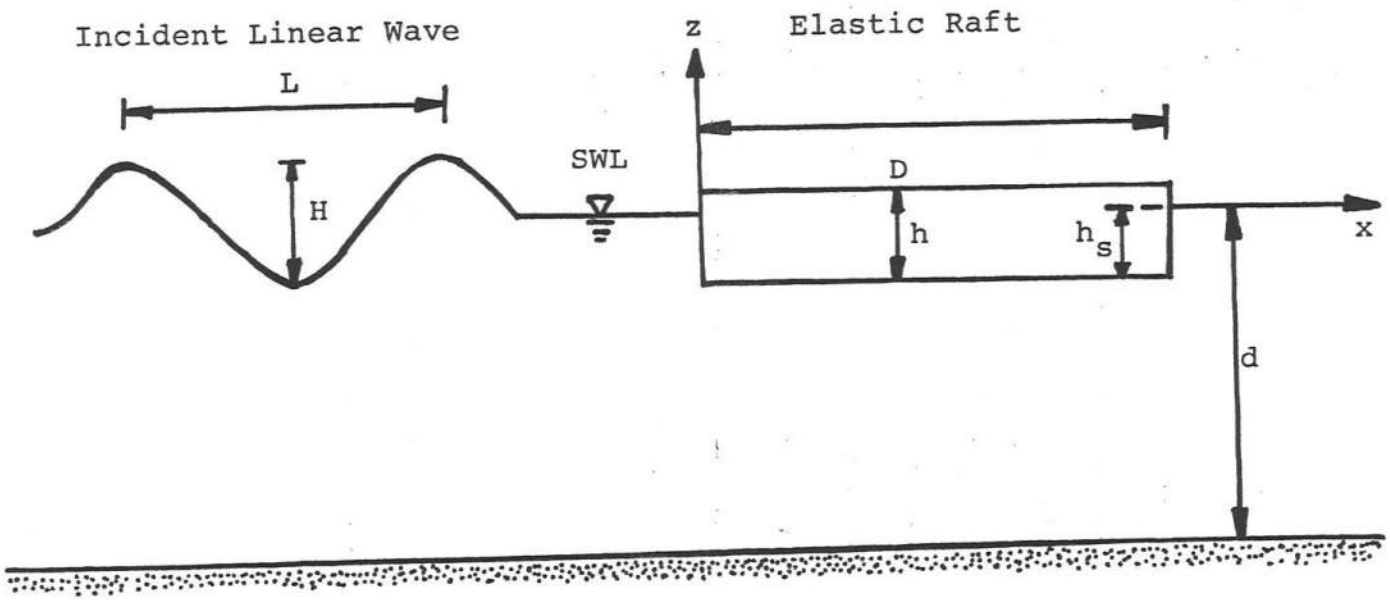

Fig. 1 - Definition Sketch for Two-Dimensional Elastic Raft Exposed to Normally-Incident Linear Wave.

The equation of the flexural motion of the thin elastic raft located in the region $0 \leq x \leq D$ as shown in Fig. 1 can be written as (e.g., Kheisin, 1967)

$$\rho_i h \frac{\partial^2 \zeta}{\partial t^2} = - D_i \frac{\partial^4 \zeta}{\partial x^4} - \rho_i g h + P_i \tag{1}$$

with $$D_i = \frac{E_i h^3}{12(1-\nu^2)} \tag{2}$$

in which ζ = vertical flexural displacement of the thin elastic raft, t = time, D_i = flexural rigidity of the ice, E_i = Young's modulus of the ice, ν = Poisson's ratio of the ice, g = gravitational acceleration, and P_i = fluid pressure underneath the ice raft at $z = (\zeta - h_s)$. The left hand side of Eq. 1 is the inertia force per unit surface area, whereas the first and second terms on the right hand side of Eq. 1 are the net vertical force per unit surface area due to the ice flexure and the weight of the ice per unit surface area, respectively. Using the Bernoulli equation (e.g., Mei, 1983) which may be linearized for the linear wave and thin elastic raft, the pressure P_i at $z = (\zeta - h_s)$ is given by

$$P_i = \rho g(h_s - \zeta) - \rho \left.\frac{\partial \Phi}{\partial t}\right|_{z=0} \tag{3}$$

in which Φ = velocity potential associated with the wave motion below the ice raft located in the region $0 \leq x \leq D$. The velocity potential Φ is defined such that the fluid velocity vector $\vec{U} = \nabla\Phi$. The first and second terms on the right hand side of Eq. 3 are the hydrostatic pressure below SWL and the dynamic pressure due to the wave motion, respectively. The dynamic pressure at $z = (\zeta - h_s)$ can be approximated by that at $z=0$ for this linearized analysis in which the vertical displacement ζ is of the order of the incident wave height H or less. Substitution of Eq. 3 into Eq. 1 together with $\rho h_s = \rho_i h$ yields

$$\rho_i h \frac{\partial^2 \zeta}{\partial t^2} = - D_i \frac{\partial^4 \zeta}{\partial x^4} - \rho g \zeta - \rho \frac{\partial \Phi}{\partial t} \Big|_{z=0} \tag{4}$$

The flexural displacement $\zeta(t,x)$ may be found as a function of t and x by solving Eq. 4 if the velocity potential below the ice raft is known. The four boundary conditions required for $\zeta(t,x)$ are that the bending moment and shear must be zero at the ice edges located at x=0 and x=D (e.g., Wadhams, 1986)

$$\frac{\partial^2 \zeta}{\partial x^2} = 0 \qquad \text{at } x=0 \text{ and } x=D \tag{5}$$

$$\frac{\partial^3 \zeta}{\partial x^3} = 0 \qquad \text{at } x=0 \text{ and } x=D \tag{6}$$

No initial conditions for $\zeta(t,x)$ are required in this analysis since the flexural motion of the ice raft will be assumed to be simple harmonic under the action of the incident linear monochromatic wave.

The velocity potential $\Phi(t,x,z)$ below the ice raft located in the region $0 \leq x \leq D$ must satisfy Laplace's equation (e.g., Mei, 1983)

$$\frac{\partial^2 \Phi}{\partial x^2} + \frac{\partial^2 \Phi}{\partial z^2} = 0 \qquad \text{in water} \tag{7}$$

The wave motion under the ice raft will also be simple harmonic since it is caused by the incident linear monochromatic wave. The kinematic boundary condition at the horizontal seabed which is assumed to be impermeable is expressed as

$$\frac{\partial \Phi}{\partial z} = 0 \qquad \text{at } z = -d \tag{8}$$

On the other hand, the kinematic boundary condition at the interface between the ice and water located at $z = (\zeta - h_s)$ is linearized in the same way as the dynamic pressure term in Eq. 3

$$\frac{\partial \zeta}{\partial t} = \frac{\partial \Phi}{\partial z} \qquad \text{at } z = 0 \tag{9}$$

Eq. 9 implies that the vertical velocity of the ice raft is the same as the vertical fluid velocity underneath the ice raft which can be evaluated at z=0 in this linearized analysis. It should be noted that the coupling between the

ice and wave motions takes place through Eqs. 4 and 9. In order to solve Eq. 7, boundary conditions at the interfaces between the ice cover and open water regions located at x=0 and D need to be specified. The matching conditions at x=0 and x=D are that the dynamic pressure and the horizontal fluid velocity must be continuous at these interfaces

$$\frac{\partial \Phi}{\partial t} \text{ is continuous} \qquad \text{at } x=0 \text{ and } x=D \tag{10}$$

$$\frac{\partial \Phi}{\partial x} \text{ is continuous} \qquad \text{at } x=0 \text{ and } x=D \tag{11}$$

Eqs. 10 and 11 imply that the wave motion in the open water regions $x \leq 0$ and $x \geq D$ need to be obtained in order to find the velocity potential below the ice raft.

The velocity potential $\Phi(t,x,z)$ in the open water regions $x \leq 0$ and $x \geq D$ must also satisfy Laplace's equation given by Eq. 7 and the kinematic boundary condition at the seabed given by Eq. 8. In the open water regions, the free water surface exposed to the atmosphere is present instead of the ice raft. However, the free surface can conveniently be regarded at a special ice cover with zero thickness h=0 and zero density ρ_i=0. Accordingly, the variable $\zeta(t,x)$ corresponds to the free surface displacement for the case of h=0 and ρ_i=0. For h=0, $h_s = (\rho_i/\rho)h = 0$ and D_i=0 according to Eq. 2. Then the linearized kinematic boundary condition at the free surface is the same as Eq. 9 with ζ = free surface displacement, while the dynamic boundary condition at the free surface is given by Eq. 4 with ρ_i=0 and D_i=0, which implies that the pressure at the free surface relative to the atmospheric pressure is zero according the Eq. 3 with h_s=0. In addition, the radiation conditions at $x=\pm\infty$ must be specified. In the far field upwave of the ice raft, the wave reflected from the ice raft must propagate in the negative x-direction, while the incident long-crest wave is specified to propagate in the positive x-

direction. In the far field downwave of the ice raft, the wave transmitted through the ice raft must propagate in the positive x-direction. It should be mentioned that the linearized two-dimensional problem formulated above is fairly general and may be applied to various problems related to the interaction of the linear wave with the thin elastic ice sheet (Kheisin, 1967; Wadhams, 1986).

2.2 General Solution for Finite Water Depth

The linearized problem formulated in Section 2.1 is solved for the case of the incident linear monochromatic wave whose velocity potential Φ_i is given by

$$\Phi_i = \text{Re}\ [\phi_i(x,z)e^{i\omega t}] \tag{12}$$

with

$$\phi_i(x,z) = \frac{igH}{2\omega} \frac{\cosh k(z+d)}{\cosh kd} e^{-ikx} \tag{13}$$

$$\omega^2 = kg \tanh kd \tag{14}$$

in which Re indicates the real part of the complex variable inside the square brackets, ϕ_i = complex function expressing the spatial variation of Φ_i, $i = \sqrt{-1}$, ω = wave angular frequency, H = incident wave height, and k = wave number. The dispersion relationship given by Eq. 14 implies that the incident wavelength $L = (2\pi/k)$ is uniquely determined for given water depth d and incident wave period $T = (2\pi/\omega)$. Eq. 12 with Eqs. 13 and 14 satisfies Laplace's equation given by Eq. 7, the kinematic boundary condition at the seabed given by Eq. 8, and the kinematic and dynamic boundary conditions at the free surface given by Eqs. 9 and 4 in which ζ = free surface displacement, $\rho_i = 0$ and $D_i = 0$.

For the incident wave described by Eq. 12, the velocity potential

$\Phi(t,x,z)$ and the displacement $\zeta(t,x)$ can be expressed as

$$\Phi = \text{Re}\ [\phi(x,z)e^{i\omega t}] \tag{15}$$

$$\zeta = \text{Re}\ [\eta(x)e^{i\omega t}] \tag{16}$$

in which ϕ = unknown complex function expressing the spatial variation of Φ, and η = unknown complex function expressing the variation of ζ with respect to x. Substitution of Eqs. 15 and 16 into Eqs. 4, 7, 8 and 9 yields

$$D_i \frac{d^4\eta}{dx^4} + (\rho g - \rho_i h\omega^2)\eta + i\rho\omega\phi\Big|_{z=0} = 0 \tag{17}$$

$$\frac{\partial^2\phi}{\partial x^2} + \frac{\partial^2\phi}{\partial z^2} = 0 \qquad \text{in water} \tag{18}$$

$$\frac{\partial\phi}{\partial z} = 0 \qquad \text{at } z = -d \tag{19}$$

$$\eta = -\frac{i}{\omega}\frac{\partial\phi}{\partial z}\Big|_{z=0} \tag{20}$$

Substituting Eq. 20 into Eq. 17, the boundary condition for ϕ at z=0 is obtained

$$D_i \frac{\partial^5\phi}{\partial z\partial x^4} + (\rho g - \rho_i h\omega^2)\frac{\partial\phi}{\partial z} - \rho\omega^2\phi = 0 \qquad \text{at } z=0 \tag{21}$$

In the region $0 \le x \le D$ below the ice cover, the complex functions $\phi(x,z)$ and $\eta(x)$ must satisfy Eqs. 18-21. On the basis of the explanations given by Kheisin (1967), a general solution of $\phi(x,z)$ below the ice cover which satisfies Eqs. 18 and 19 may be expressed in the form

$$\phi = \frac{igH}{2\omega\ \cosh(kd)} \left\{ \sum_{n=1}^{3} (A_n e^{iK_n x} + B_n e^{-iK_n x})\ \cosh\ [K_n(z+d)] \right.$$

$$\left. + \sum_{n=4}^{\infty} (A_n e^{K_n x} + B_n e^{-K_n x})\ \cos\ [K_n(z+d)] \right\} \tag{22}$$

in which K_n = wave numbers explained below, and A_n and B_n = unknown complex constants which need to be determined using the boundary conditions with respect to x. The dispersion relationship for K_n in Eq. 22 is obtained by

substituting Eq. 22 into Eq. 21. K_n with n=1, 2 and 3 must satisfy the following equation

$$D_i K_n^5 + (\rho g - \rho_i h\omega^2) K_n - \frac{\rho\omega^2}{\tanh(K_n d)} = 0 \qquad (n=1,2,3) \tag{23}$$

Eq. 23 has three roots in which $K_1>0$, $K_2 = (K_r + iK_i)$ and $K_3 = (K_r - iK_i)$ with K_r and K_i being real positive. On the other hand, K_n with n=4, 5, ..., ∞ are an infinite number of real positive roots, i.e., $K_n>0$ of the following equation

$$D_i K_n^5 + (\rho g - \rho_i h\omega^2) K_n + \frac{\rho\omega^2}{\tan(K_n d)} = 0 \qquad (n=4,5,\ldots) \tag{24}$$

Substituting Eq. 22 to Eq. 20, the complex function $\eta(x)$ related to the vertical displacement of the ice cover is expressed as

$$\eta = \frac{H}{2k \sinh(kd)} \left[\sum_{n=1}^{3} K_n \sinh(K_n d) \left(A_n e^{iK_n x} + B_n e^{-iK_n x}\right) - \sum_{n=4}^{\infty} K_n \sin(K_n d) \left(A_n e^{K_n x} + B_n e^{-K_n x}\right) \right] \tag{25}$$

in which use is made of Eq. 14.

In the open water regions $x\leq 0$ and $x\geq D$, the complex functions $\phi(x,z)$ and $\eta(x)$ must also satisfy Eqs. 18-21 except that $D_i=0$ and $\rho_i=0$ in Eq. 21. A general solution of $\phi(x,z)$ can be expresses in the form (e.g., Mei, 1983)

$$\phi = \frac{igH}{2\omega \cosh(kd)} \left\{ \left(a_1 e^{ik_1 x} + b_1 e^{-ik_1 x}\right) \cosh[k_1(z+d)] + \sum_{n=2}^{\infty} \left(a_n e^{k_n x} + b_n e^{-k_n x}\right) \cos[k_n(z+d)] \right\} \tag{26}$$

in which k_n (n=1,2,...) = wave numbers explained below, and a_n and b_n (n=1,2,...) = unknown complex constants which need to be determined using the boundary conditions with respect to x. The dispersion relationship for k_n in Eq. 26 is obtained by substituting Eq. 26 into Eq. 21 with $D_i = 0$ and $\rho_i = 0$.

k_1 is the real positive root of the following equation

$$k_1 g \tanh(k_1 d) = \omega^2 \tag{27}$$

Comparison between Eqs. 14 and 27 indicates that $k_1 = k$ is the wave number of the incident linear wave expressed by Eq. 12. k_n with n=2,3,..., ∞ are an infinite number of real positive roots, i.e., $k_n>0$ of the following equation

$$k_n g \tan(k_n d) = -\omega^2 \qquad (n=2,3,\ldots) \tag{28}$$

Substituting Eq. 26 into Eq. 20, the complex function $\eta(x)$ related to the free surface displacement is given by

$$\eta = \frac{H}{2k \sinh(kd)} \left[k_1 \sinh(k_1 d) \left(a_1 e^{ik_1 x} + b_1 e^{-ik_1 x}\right) - \sum_{n=2}^{\infty} k_n \sin(k_n d) \left(a_n e^{k_n x} + b_n e^{-k_n x}\right)\right] \tag{29}$$

It may be apparent that Eqs. 26-29 for the open water with $D_i=0$ and $\rho_i=0$ correspond to Eqs. 22-25 for the ice cover region, respectively.

In order to find the complex constants A_n, B_n, a_n and b_n, the general solutions for the open water and ice cover regions need to be matched. First, in the region $x\leq 0$ upwave of the ice raft, ϕ and η are given by Eqs. 26 and 29, respectively, without regard to the boundary conditions with respect to x. The functions ϕ and η which satisfy the radiation condition at $x = -\infty$ are given by

$$\phi_1 = \frac{igH}{2\omega \cosh(kd)} \left\{\left(a_1 e^{ik_1 x} + e^{-ik_1 x}\right) \cosh\left[k_1(z+d)\right] + \sum_{n=2}^{N_1} a_n e^{k_n x} \cos\left[k_n(z+d)\right]\right\} \tag{30}$$

$$\eta_1 = \frac{H}{2k \sinh(kd)} \left[k_1 \sinh(k_1 d) \left(a_1 e^{ik_1 x} + e^{-ik_1 x}\right) - \sum_{n=2}^{N_1} k_n \sin(k_n d)\, a_n e^{k_n x}\right] \tag{31}$$

in which ϕ_1 and η_1 = functions ϕ and η in the region $x \leq 0$, and N_1 = number of terms in the infinite series retained for the actual computation. In Eqs. 30 and 31, k_1 and k_n $(n=2,3,\ldots,N_1)$ need to be found from Eqs. 27 and 28, respectively, for given g, d and ω. Comparison between Eqs. 13 and 30 shows that the term involving $\exp(-ik_1x)$ with $k_1 = k$ in Eq. 30 represents the incident linear wave whose height is given by H. The term related to the complex constant a_1 represnts the reflected wave propagating in the negative x-direction and the wave reflection coefficient $R = |a_1|$ which is a positive value. The evanescent terms associated with a_n $(n=2,3,\ldots)$ decay exponentially as $x \to -\infty$ since $k_n > 0$. Second, in the region $0 \leq x \leq D$ of the ice raft, ϕ and η are given by Eqs. 22 and 25, respectively, which are approximated by

$$\phi_2 = \frac{igH}{2\omega \cosh(kd)} \left\{ \sum_{n=1}^{3} (A_n e^{iK_n x} + B_n e^{-iK_n x}) \cosh[K_n(z+d)] + \sum_{n=4}^{N_2} (A_n e^{K_n x} + B_n e^{-K_n x}) \cos[K_n(z+d)] \right\} \tag{32}$$

$$\eta_2 = \frac{H}{2k \sinh(kd)} \left[\sum_{n=1}^{3} K_n \sinh(K_n d) (A_n e^{iK_n x} + B_n e^{-iK_n x}) - \sum_{n=4}^{N_2} K_n \sin(K_n d) (A_n e^{K_n x} + B_n e^{-K_n x}) \right] \tag{33}$$

in which ϕ_2 and η_2 = functions ϕ and η in the region $0 \leq x \leq D$, and N_2 = number of terms retained for the computation. $K_n(n=1,2,\ldots,N_2)$ in Eqs. 32 and 33 must be obtained from Eqs. 23 and 24 for given ρ, g, ρ_i, h, D_i, d and ω. Third, in the region $x \geq D$ downwave of the ice raft, the functions ϕ and η expressed in the form of Eqs. 26 and 29 need to satisfy the radiation condition at $x=\infty$ and can be written as

$$\phi_3 = \frac{igH}{2\omega \cosh(kd)} \left\{ b_1 e^{-ik_1 x} \cosh[k_1(z+d)] + \sum_{n=2}^{N_3} b_n e^{-k_n x} \cos[k_n(z+d)] \right\} \tag{34}$$

$$\eta_3 = \frac{H}{2k \sinh(kd)} \left[k_1 \sinh(k_1 d)\, b_1 e^{-ik_1 x} - \sum_{n=2}^{N_3} k_n \sin(k_n d)\, b_n e^{-k_n x} \right] \tag{35}$$

in which N_3 = number of terms used for the computation. In Eqs. 34 and 35, the term associated with the complex constant b_1 represents the transmitted wave propagating in the positive x-direction, while the evanescent terms associated with b_n (n=2,3,...) decay exponentially as $x \to \infty$. Since $k_1 = k$ in Eqs. 34 and 35, the wave transmission coefficient $T_r = |b_1|$ which is a real positive value.

The $(N_1 + 2N_2 + N_3)$ unknown constants a_n, A_n, B_n and b_n in Eqs. 30-35 are determined to satisfy the conditions at x=0 and D given by Eqs. 5, 6, 10 and 11. Eq. 5 reduces to $\partial^2 \eta_2 / \partial x^2 = 0$ at x=0 and x=D with η_2 given by Eq. 33 and requires

$$\sum_{n=1}^{3} K_n^3 \sinh(K_n d)\,(A_n + B_n) + \sum_{n=4}^{N_2} K_n^3 \sin(K_n d)(A_n + B_n) = 0 \tag{36}$$

$$\sum_{n=1}^{3} K_n^3 \sinh(K_n d)(A_n e^{iK_n D} + B_n e^{-iK_n D}) + \sum_{n=4}^{N_2} K_n^3 \sin(K_n d)\,(A_n e^{K_n D} + B_n e^{-K_n D}) = 0 \tag{37}$$

Eq. 6 results in $\partial^3 \eta_2 / \partial x^3 = 0$ at x=0 and x=D from which we obtain

$$\sum_{n=1}^{3} iK_n^4 \sinh(K_n d)\,(A_n - B_n) + \sum_{n=4}^{N_2} K_n^4 \sin(K_n d)\,(A_n - B_n) = 0 \qquad (38)$$

$$\sum_{n=1}^{3} iK_n^4 \sinh(K_n d)\,(A_n e^{iK_n D} - B_n e^{-iK_n D}) + \sum_{n=4}^{N_2} K_n^4 \sin(K_n d)\,(A_n e^{K_n D} - B_n e^{-K_n D}) = 0 \qquad (39)$$

On the other hand, the matching conditions expressed by Eqs. 10 and 11 require

$$\phi_1 = \phi_2 \quad ; \quad \frac{\partial \phi_1}{\partial x} = \frac{\partial \phi_2}{\partial x} \qquad \text{at } x = 0 \qquad (40)$$

$$\phi_2 = \phi_3 \quad ; \quad \frac{\partial \phi_2}{\partial x} = \frac{\partial \phi_3}{\partial x} \qquad \text{at } x = D \qquad (41)$$

Eqs. 40 and 41 must be satisfied at any value of z in the region $-d \le z \le 0$. For the computation, the matching conditions given in Eqs. 40 and 41 are satisfied at the specified vertical locations z_i (i=1,2,...,I) at x=0 and z_j (j=1.2,...,J) at x=D. As a result, Eq. 40 yields the following 2I equations

$$(a_1 + 1)\cosh[k_1(z_i + d)] + \sum_{n=2}^{N_1} a_n \cos[k_n(z_i + d)] = \sum_{n=1}^{3} (A_n + B_n)\cosh[K_n(z_i+d)] + \sum_{n=4}^{N_2} (A_n + B_n)\cos[K_n(z_i + d)] \qquad (42)$$

$$ik_1 (a_1 - 1)\cosh[k_1(z_i + d)] + \sum_{n=2}^{N_1} k_n a_n \cos[k_n(z_i+d)] = \sum_{n=1}^{3} iK_n (A_n - B_n)\cosh[K_n(z_i+d)] + \sum_{n=4}^{N_2} K_n (A_n - B_n)\cos[K_n(z_i+d)] \qquad (43)$$

Likewise, Eq. 41 results in the following 2J equations

$$\sum_{n=1}^{3} (A_n e^{iK_nD} + B_n e^{-iK_nD}) \cosh [K_n(z_j+d)]$$

$$+ \sum_{n=4}^{N_2} (A_n e^{K_nD} + B_n e^{-K_nD}) \cos[K_n(z_j+d)] = b_1 e^{-ik_1D} \cosh[k_1(z_j+d)]$$

$$+ \sum_{n=2}^{N_3} b_n e^{-k_nD} \cos[k_n(z_j+d)] \qquad (44)$$

$$\sum_{n=1}^{3} iK_n(A_n e^{iK_nD} - B_n e^{-iK_nD}) \cosh [K_n(z_j+d)]$$

$$+ \sum_{n=4}^{N_2} K_n (A_n e^{K_nD} - B_n e^{-K_nD}) \cos [K_n(z_j+d)]$$

$$= -ik_1 b_1 e^{-ik_1D} \cosh[k_1(z_j+d)]$$

$$- \sum_{n=2}^{N_3} k_n b_n e^{-k_nD} \cos[k_n(z_j+d)] \qquad (45)$$

Eqs. 36-39 and 42-45 may be rearranged in a matrix form and solved to obtain the unknown constants a_n $(n=1,2,\ldots,N_1)$, $A_n(n=1,2,\ldots,N_2)$, $B_n(n=1,2,\ldots,N_2)$ and $b_n(n=1,2,\ldots,N_3)$. In order to uniquely determine these unknown values, the following relationship must be satisfied

$$N_1 + 2N_2 + N_3 = 4 + 2I + 2J \qquad (46)$$

For the actual computation, the values of N_1, N_2, N_3, I and J should be selected on the basis of the degree of accuracy required for specific applications.

2.3 Wave Drift Force on a Two-Dimensional Floe

Once the constants a_n, A_n, B_n and b_n are found, various quantities of interest can be obtained using Eqs. 30-35. The flexural oscillation of the ice raft can be investigated using Eq. 33. The wave reflection and

transmission coefficients are given by

$$R = |a_1| \quad ; \quad T_r = |b_1| \tag{47}$$

in which a_1 and b_1 = complex constants.

The incident waves exert oscillatory and drift forces on the ice raft. The wave drift force averaged over the wave period should be included in the ice floe force balance used for predicting the horizontal movement of the ice floes in partially ice-covered waters (Madsen et al., 1986; Kobayashi et al., 1987). For a two-dimensional body in normally incident waves, the mean wave drift force per unit width, F_d, acts in the direction of the wave propagation and is given by (Longuet-Higgins, 1977)

$$F_d = \frac{1}{16} \rho g H^2 \left[1 + \frac{2kd}{\sinh(2kd)}\right] (1 + R^2 - T_r^2) \tag{48}$$

in which F_d is proportional to H^2 but the mean second-order drift force depends on the first-order quantities only. Since no wave energy absorption and dissipation will occur for the potential flow and elastic ice assumed in the present analysis, the conservation of wave energy requires (e.g., Mei, 1983)

$$R^2 + T_r^2 = 1 \tag{49}$$

in which $0 \leq R \leq 1$ and $0 \leq T_r \leq 1$. Substitution of Eq. 49 into Eq. 48 yields

$$F_d = \frac{1}{8} \rho g H^2 R^2 \left[1 + \frac{2kd}{\sinh(2kd)}\right] \tag{50}$$

In order to compare the wave drift force on the two-dimensional ice raft to that on a three-dimensional ice floe, it is convenient to introduce the normalized wave drift force defined by

$$f_d = \frac{F_d}{\rho g H^2} = \frac{1}{8} R^2 \left[1 + \frac{2kd}{\sinh(2kd)}\right] \tag{51}$$

In deep water for which (d/L) > 0.5, that is, (kd) > π, (2kd)/sinh(2kd) << 1 (e.g., U.S. Army Coastal Engineering Research Center, 1984). In deep water, Eqs. 50 and 51 can hence be approximated by

$$F_d = \frac{1}{8} \rho g H^2 R^2 \qquad \text{in deep water} \qquad (52)$$

$$f_d = \frac{1}{8} R^2 \qquad \text{in deep water} \qquad (53)$$

It should be mentioned that the analysis of Longuet-Higgins (1977) assumed the existence of the difference in the mean surface levels between the up-wave and down-wave sides. This assumption may not be appropriate in open water far from the coastline but the assumed mean surface level difference is negligible in deep water.

2.4 Approximate Solution for Deep Water Depth

The problem formulated for finite water depth in Section 2.2 requires significant computational efforts. In deep water, the problem becomes independent of the water depth d and can be simplified considerably. For (kd)>π, the dispersion relationship for the open water given by Eq. 27 with k_1=k reduces to

$$k_1 g = \omega^2 \qquad (54)$$

Moreover, there are no evanescent modes in deep water and Eq. 28 for k_n with n $\geq$ 2 is not required. Likewise, the dispersion relationship for the ice cover region expressed by Eq.23 is simplified as

$$D_i K_n^5 + (\rho g - \rho_i h \omega^2) K_n - \rho \omega^2 = 0 \qquad (n=1,2,3) \qquad (55)$$

Eq. 24 for K_n with n $\geq$ 4 is not needed for deep water depth since Eq. 55 has no equation similar to Eq. 24 corresponding to Eq. 23. As a result, only the terms involving k_1, K_1, K_2 and K_3 exist for deep water depth.

Accordingly, in deep water, the solutions given by Eqs. 30-35 for finite water depth are modified as

$$\phi_1 = \frac{igH}{2\omega}\left(a_1 e^{ik_1 x} + e^{-ik_1 x}\right) e^{k_1 z} \tag{56}$$

$$\eta_1 = \frac{H}{2}\left(a_1 e^{ik_1 x} + e^{-ik_1 x}\right) \tag{57}$$

$$\phi_2 = \frac{igH}{2\omega}\sum_{n=1}^{3}\left(A_n e^{iK_n x} + B_n e^{-iK_n x}\right) e^{K_n z} \tag{58}$$

$$\eta_2 = \frac{H}{2k_1}\sum_{n=1}^{3} K_n\left(A_n e^{iK_n x} + B_n e^{-iK_n x}\right) \tag{59}$$

$$\phi_3 = \frac{igH}{2\omega}\, b_1 e^{-ik_1 x}\, e^{k_1 z} \tag{60}$$

$$\eta_3 = \frac{H}{2}\, b_1\, e^{-ik_1 x} \tag{61}$$

Eqs. 56, 58 and 60 satisfy Eq. 18 and Eq. 19 with $d \to \infty$ where $k = k_1 > 0$, $K_1 > 0$, $\mathrm{Re}[K_2] = \mathrm{Re}[K_3] = K_r > 0$. Eq. 20 can also be shown to be satisfied. Substitution of Eq. 58 into Eq. 21 yields Eq. 55, while substitution of Eq. 56 or 60 into Eq. 21 with $D_i = 0$ and $\rho_i = 0$ results in Eq. 54. Eqs. 56 and 57 satisfy the radiation condition at $x = -\infty$, whereas Eqs. 60 and 61 satisfy the radiation condition at $x = \infty$. As a result, the unknown complex constants a_1, A_n (n=1,2,3), B_n (n=1,2,3) and b_1 in Eqs. 56-61 need to be found using the conditions required at $x = 0$ and $x = D$.

The equations for deep water depth corresponding to Eqs. 36-39 are written as

$$\sum_{n=1}^{3} K_n^3 (A_n + B_n) = 0 \tag{62}$$

$$\sum_{n=1}^{3} K_n^3 (A_n e^{iK_n D} + B_n e^{-iK_n D}) = 0 \tag{63}$$

$$\sum_{n=1}^{3} K_n^4 \, (A_n - B_n) = 0 \tag{64}$$

$$\sum_{n=1}^{3} K_n^4 (A_n e^{iK_n D} - B_n e^{-iK_n D}) = 0 \tag{65}$$

Eqs. 62-65 ensure that the boundary conditions given by Eqs. 5 and 6 are satisfied in deep water. Furthermore, the matching conditions expressed by Eqs. 40 and 41 must be satisfied at any value of z in the region $z \leq 0$ at $x = 0$ and $x = D$. However, the deep water solutions given by Eqs. 56-61 with no evanescent modes can satisfy these matching conditions only at one value of z and are hence only approximate. Squire (1984a) and Wadhams (1986) matched the solutions at $z = 0$ only since the wave action tends to decrease downward from $z = 0$. Making the same approximation, Eqs. 40 and 41 are satisfied at $z = 0$ only

$$a_1 - \sum_{n=1}^{3} (A_n + B_n) = -1 \tag{66}$$

$$k_1 a_1 - \sum_{n=1}^{3} K_n \, (A_n - B_n) = k_1 \tag{67}$$

$$\sum_{n=1}^{3} (A_n e^{iK_n D} + B_n e^{-iK_n D}) - b_1 e^{-ik_1 D} = 0 \tag{68}$$

$$\sum_{n=1}^{3} K_n \, (A_n e^{iK_n D} - B_n e^{-iK_n D}) + k_1 b_1 e^{-ik_1 D} = 0 \tag{69}$$

Solving the eight linear equations given by Eqs. 62-69, the values of a_1, A_n (n=1,2,3), B_n (n=1,2,3) and b_1 can be found. The wave reflection and transmission coefficients can be calculated using Eq. 47, while the wave drift force per unit width can be found using Eq. 52. Furthermore, the vertical displacement of the ice raft is given by $\mathrm{Re}[\eta_2(x) \exp(i\omega t)]$ in the region

$0 \leq x \leq D$ in which η_2 is expressed by Eq. 59. Consequently, the amplitude of the ice displacement is equal to $|\eta_2(x)|$ which may be normalized by the amplitude of the incident linear wave given by (H/2)

$$\eta_m(x) = \frac{2|\eta_2(x)|}{H} = \frac{1}{k_1} \left| \sum_{n=1}^{3} K_n \left(A_n e^{iK_n x} + B_n e^{-iK_n x} \right) \right| \tag{70}$$

in which η_m = normalized amplitude of the ice displacement in the region $0 \leq x \leq D$.

2.5 Computation Procedure

The computation procedure for the approximate solution for deep water depth presented in Section 2.4 is explained in the following. The input parameters required for the computation are: ρ = density of the water, g = gravitational acceleration, ρ_i = density of the ice, E_i = Young's modulus of the ice, ν = Poisson's ratio of the ice, h = thickness of the ice, D = width of the ice raft, and T = incident wave period. The incident wave height, H, is not specified since only the normalized quantities are computed herein. The flexural rigidity of the ice, D_i, is calculated using Eq. 2. The incident wave number $k = k_1 = (\omega^2/g)$ from Eq. 54 in which $\omega = (2\pi/T)$ = wave angular frequency. The incident wavelength, L, is defined as $L = (2\pi/k)$.

Eq. 55 is then solved to obtain K_1, K_2 and K_3 in which K_1 is a real positive value, and K_2 and K_3 are complex conjugates

$$K_2 = K_r + iK_i \quad ; \quad K_3 = K_r - iK_i \tag{71}$$

where $K_r > 0$ and $K_i > 0$. It should be noted that K_r must be positive to ensure that ϕ_2 given by Eq. 58 approaches zero as $z \to (-\infty)$. First, K_1 is computed from

$$K_1^5 + C_1 K_1 - C_2 = 0 \tag{72}$$

with

$$C_1 = \frac{\rho g - \rho_i h \omega^2}{D_i} \quad ; \quad C_2 = \frac{\rho \omega^2}{D_i} > 0 \tag{73}$$

It can be shown that Eq. 72 with $C_2 > 0$ has only one positive root. Eq. 72 is solved using a Newton-Raphson iteration method (e.g., Abramowitz et al., 1972) starting from $K_1 = k$. The other roots of Eq. 55 are the roots of the following equation

$$u^4 + u^3 + u^2 + u + C_3 = 0 \tag{74}$$

with

$$u = \frac{K_n}{K_1} \quad ; \quad C_3 = \frac{C_2}{K_1^5} > 0 \tag{75}$$

in which $K_n = uK_1$ and K_1 is the real positive value obtained above. Eq. 74 can be separated into the following two quadratic equations

$$u^2 + C_4 u + C_5 = 0 \tag{76}$$

$$u^2 + C_6 u + C_7 = 0 \tag{77}$$

with

$$C_4 = \frac{1}{2} - \left(v - \frac{3}{4}\right)^{1/2} \tag{78}$$

$$C_5 = \begin{cases} \frac{v}{2} + \left(\frac{v^2}{4} - C_3\right)^{1/2} & \text{for } v \le 2 \\ \frac{v}{2} - \left(\frac{v^2}{4} - C_3\right)^{1/2} & \text{for } v > 2 \end{cases} \tag{79}$$

$$C_6 = \frac{1}{2} + \left(v - \frac{3}{4}\right)^{1/2} \tag{80}$$

$$C_7 = \begin{cases} \frac{v}{2} - \left(\frac{v^2}{4} - C_3\right)^{1/2} & \text{for } v \le 2 \\ \frac{v}{2} + \left(\frac{v^2}{4} - C_3\right)^{1/2} & \text{for } v > 2 \end{cases} \tag{81}$$

in which the variable v is the real root of the following equation which satisfies the conditions of $v > 1$ and $v > 2\sqrt{C_3}$

$$v^3 - v^2 + (1 - 4C_3)\, v + (3C_3 - 1) = 0 \tag{82}$$

It can be shown that Eq. 82 has only one real root which is greater than unity and $2\sqrt{C_3}$. Eq. 82 is solved using a Newton-Raphson iteration method starting from $v = \max(1, 2\sqrt{C_3})$. Since $v > 1$ and $v > 2\sqrt{C_3}$, hence $C_4 < 0$, $C_5 > 0$, $C_6 > 0$ and $C_7 > 0$. Solving Eq. 76, K_2 and K_3 are expressed as

$$K_2 = \frac{1}{2}\, K_1 \left[- C_4 + i\, (4C_5 - C_4^2)^{\frac{1}{2}} \right] \tag{83}$$

$$K_3 = \frac{1}{2}\, K_1 \left[- C_4 - i\, (4C_5 - C_4^2)^{\frac{1}{2}} \right] \tag{84}$$

where it can be shown that $(4C_5 - C_4^2) > 0$. Comparison of Eqs. 83 and 84 with Eq. 71 indicates

$$K_r = - \frac{1}{2}\, K_1\, C_4 > 0 \tag{85}$$

$$K_i = \frac{1}{2}\, K_1 (4C_5 - C_4^2)^{\frac{1}{2}} > 0 \tag{86}$$

On the other hand, Eq. 77 yields two roots whose real parts are negative since $C_6 > 0$ and $C_7 > 0$. These roots are discarded since ϕ_2 given by Eq. 58 will approach infinity as $z \to (-\infty)$ if Re $[K_n] < 0$.

After K_1, K_2 and K_3 are computed, the complex coefficients for the eight linear equations given by Eqs. 62-69 for the unknown values of a_1, $A_n (n=1,2,3)$, $B_n (n=1,2,3)$ and b_1 are calculated. The solution of the eight complex linear equations is obtained using the external subroutine LEQT1C in IMSL library. Then, the reflection and transmission coefficients are calculated using Eq. 47, while the normalized wave drift force, which is independent of the incident wave height H, is obtained using Eq. 53. Moreover, the normalized amplitude of the ice displacement expressed by Eq. 70 is computed as a function of x in the range $0 \le x \le D$.

3.0 RIGID ICE FLOES

In this section, an ice floe is assumed to be rigid and vertically axisymmetric. The response of the three-dimensional ice floe of finite thickness under the action of incident linear waves is analyzed by computing the linear waves scattered and radiated by the ice floe. The motion of the rigid floe is separated into the three oscillatory modes corresponding to surge, heave and pitch and the wave-induced drift. The numerical method described in this report is based on that used by Kobayashi et al. (1986, 1987) and Frankenstein (1986) who made example computations for the oscillatory motions of the ice floe and the wave drift force acting on the ice floe. The numerical method is limited to a single ice floe although it could be extended to multiple floes with significant additional computational efforts (Kagemoto et al., 1986).

3.1 Wave Diffraction and Radiation

The computation methods for linear wave diffraction and radiation by a floating rigid body are well established (Mei, 1983). For vertical axisymmetric bodies including cylinders and spheres, the use of an axisymmetric Green's function method reduces the required computational effort significantly (Eatock Taylor et al., 1978; Fenton, 1978; Isaacson, 1982). Consequently, the ice mass examined in the following is assumed to be rigid and vertically axisymmetric. The associated wave field is assumed to be given by linear potential flow theory. The effect of flow separation for a floating small ice mass is expected to be negligible in the absence of winds and currents since the small ice mass behaves approximately as a fluid particle (Lever et al., 1984). The use of linear wave theory will be valid if the wave

height, H, is small relative to the wavelength, L, and the water depth, d, which is assumed to be constant. Furthermore, the incident wave is assumed to be regular and long-crested. The present linear analysis could be extended to the case of random incident waves (Løken et al., 1979; Pinkster et al., 1983) if the random wave characteristics in partially ice-covered waters are known.

The problem analyzed here is illustrated in Fig. 2 where the Cartesian coordinate system (x,y,z) used in the analysis is defined. The x-axis is taken to be positive in the direction of incident wave propagation, whereas the z-axis is positive vertically upwards from the still water level. The rigid body shown in Fig. 2 is vertically axisymmetric about the z-axis and oscillates under the action of the incident linear wave. The translational motions in the x and z directions are termed surge and heave, respectively, while the rotational motion about the y-axis is termed pitch (Isaacson, 1982). The velocity potential, Φ, defined such that the fluid velocity vector $\vec{U} = \nabla\Phi$, is expressed as

$$\Phi = \mathrm{Re}[\phi(x,y,z)e^{i\omega t}] \tag{87}$$

in which t = time, ω = angular frequency, ϕ = complex function expressing the spatial variation of Φ and Re indicates the real part of the complex variable inside the square brackets. The following analysis is essentially based on the mathematical formulations given by Eatock Taylor et al. (1978), Isaacson (1982) and Mei (1983) although they did not compute the wave and ice interaction. Since Isaacson and Mei used $\exp(-i\omega t)$ in Eq. 87, ϕ in their analyses corresponds to the complex conjugate of ϕ in the present analysis and that of Eatock Taylor et al.

The velocity potential expressed in Eq. 87 needs to satisfy the Laplace

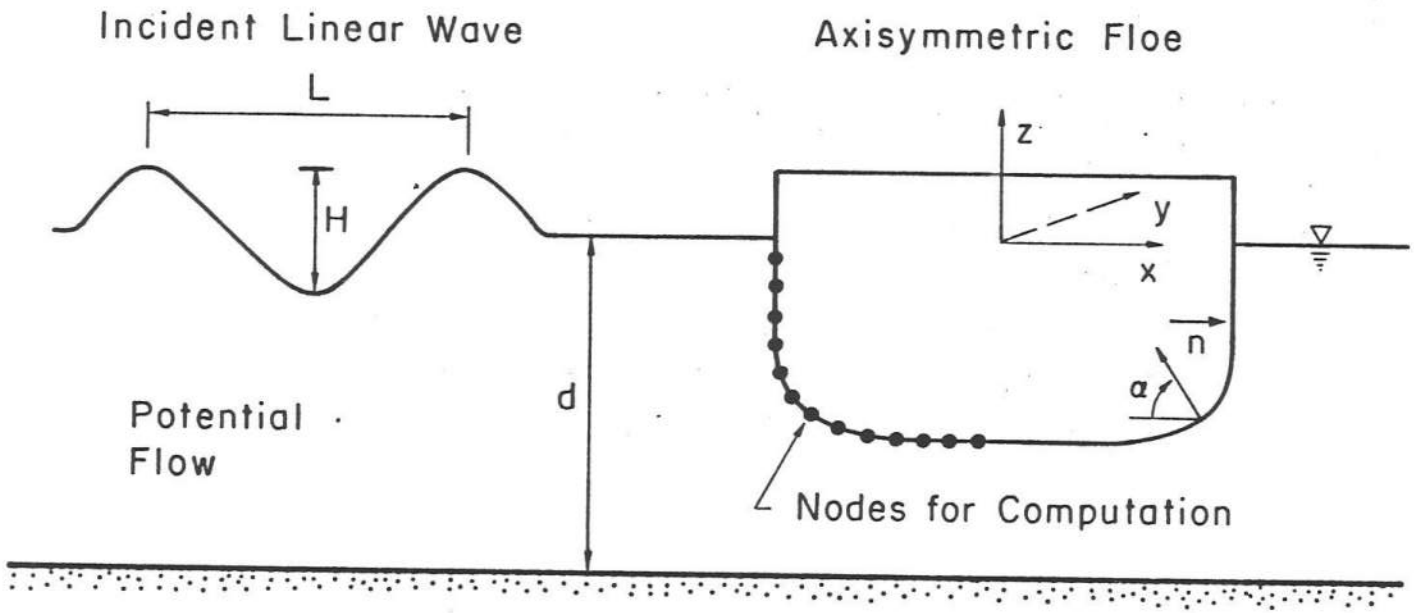

Fig. 2 - Definition Sketch for Vertically Axisymmetric Floe Exposed to Incident Linear Wave.

equation in the fluid domain, the kinematic boundary condition at the horizontal seabed, the linearized kinematic and dynamic boundary conditions at the free surface, the radiation condition at the far field and the linearized kinematic boundary condition at the submerged surface of the body at rest (e.g., Mei, 1983). The last boundary condition implies that the fluid velocity in the direction of the unit normal vector, $\vec{n}_o$, which is taken to be positive inward into the body, equals the velocity of the submerged surface in the same direction arising from the surge, heave and pitch motions. Accordingly, the complex function ϕ can be separated into (Isaacson, 1982)

$$\phi = \phi_i + \phi_s + \sum_{j=1}^{3} \phi_j \, \xi_j \tag{88}$$

in which the subscripts i and s indicate the incident and scattered waves associated with the stationary body and the subscripts j=1,2 and 3 denote the surge, heave and pitch motions, respectively. In Eq. 88, ξ_j is the complex amplitude of each of the surge, heave and pitch motions expressed in the form $\xi_j \exp(i\omega t)$ and ϕ_j is the complex function associated with each of the body motions for the case of $\xi_j = 1$. The boundary conditions at the submerged surface of the body at rest thus become independent of ξ_j and are given by Isaacson (1982) who took the unit normal vector $\vec{n}_o$ to be positive outward from the body.

As a result, the boundary-value problem for each of the unknown complex functions ϕ_s and ϕ_j(j=1,2 and 3) can be solved separately first. Then, the equations for the surge, heave and pitch motions can be solved to obtain the unknown complex amplitudes ξ_j(j=1,2 and 3).

3.2 Boundary Integral Equations

Using Green's theorem, the following surface integral equation for ϕ_j with j=1,2,3 or 4, where the subscript j=4 is used to represent the subscript s, can be derived (Mei, 1983)

$$\epsilon\ \phi_j(\vec{x}) = \iint_{S_B}\left[\phi_j(\vec{x}_o)\ \frac{\partial G(\vec{x}|\vec{x}_o)}{\partial n_o} - G(\vec{x}|\vec{x}_o)\ \frac{\partial \phi_j(\vec{x}_o)}{\partial n_o}\right] dS_B \tag{89}$$

in which S_B = submerged surface of the body at rest, n_o = distance in the direction of the unit normal vector, and $G(\vec{x}|\vec{x}_o)$ = Green's function related to the potential at any field point $\vec{x} = (x,y,z)$ due to an oscillating source of unit strength at the point $\vec{x}_o = (x_o, y_o, z_o)$ on S_B (Mei, 1983). The parameter ϵ in Eq. 89 is given by $\epsilon = 1$ or 1/2 depending on whether the point $\vec{x}$ is located in the fluid domain or on S_B, respectively. It should be mentioned that Fenton (1978) and Isaacson (1982) used a closely related method based on a source strength distribution function instead of Eq. 89.

For a vertical axisymmetric body, it is convenient to use the cylindrical coordinate system $(r,\theta\ z)$ with $x = r\cos\theta$ and $y = r\sin\theta$ and express ϕ_j (j=1,2,3 or 4) in terms of Fourier series with respect to angle θ

$$\phi_j(\vec{x}) = \phi_j^o(r,z) + 2\sum_{m=1}^{\infty} \phi_j^m(r,z)\cos(m\theta) \tag{90}$$

where ϕ_j^m(m=0,1,2...) is the unknown complex function which depends on the two-dimensional coordinate system (r,z) in the vertical plane. Eq. 90 indicates that ϕ_j is symmetric about the axis of θ=0, that is, the x-axis. Correspondingly, the Green's function can be expressed as

$$G(\vec{x}|\vec{x}_o) = G^o(r,z|r_o,z_o) + 2\sum_{m=1}^{\infty} G^m(r,z|r_o,z_o)\cos[m(\theta-\theta_o)] \tag{91}$$

in which the complex function G^m(m=0,1,2...) depending on r, z, r_o and z_o with

$x_o = r_o\cos\theta_o$ and $y_o = r_o \sin\theta_o$ was given by Fenton (1978) and consists of the propagating mode and evanescent modes.

Substituting Eqs. 90 and 91 into Eq. 89 and integrating the resulting equation with respect to θ_o, the following line integral equation for $\phi_j^m(r,z)$ can be derived (Eatock Taylor et al., 1978)

$$\frac{\epsilon}{2\pi}\,\phi_j^m(r,z) = \int_{L_B}\left[\phi_j^m(r_o,\, z_o)\;\frac{\partial G^m(r,z|r_o,z_o)}{\partial n_o} - G^m(r,z|r_o,z_o)\frac{\partial \phi_j^m(r_o,z_o)}{\partial n_o}\right] r_o dL_B \tag{92}$$

in which L_B is the contour of the submerged body surface in the vertical plane and the point $(r_o,\, z_o)$ is located on this contour. In Eq. 92, the variations of $\phi_j^m(r_o,z_o)$ (j=1,2,3 or 4 and m=0,1,2,...) on L_B are unknown but their normal derivatives on L_B can be found from the kinematic boundary condition at the submerged body surface (Isaacson, 1982)

$$\frac{\partial \phi_1^m(r_o,z_o)}{\partial n_o} = \begin{cases} -\frac{i}{2}\,\omega\,\cos\alpha & m=1 \\ 0 & \text{otherwise} \end{cases} \tag{93}$$

$$\frac{\partial \phi_2^m(r_o,z_o)}{\partial n_o} = \begin{cases} i\omega\,\sin\alpha & m=0 \\ 0 & \text{otherwise} \end{cases} \tag{94}$$

$$\frac{\partial \phi_3^m(r_o,z_o)}{\partial n_o} = \begin{cases} -\frac{i}{2}\,\omega\,(z_o\,\cos\alpha + r_o\,\sin\alpha) & m=1 \\ 0 & \text{otherwise} \end{cases} \tag{95}$$

$$\frac{\partial \phi_s^m(r_o,z_o)}{\partial n_o} = \cos\alpha\,\frac{\partial \phi_i^m(r_o,z_o)}{\partial r_o} - \sin\alpha\,\frac{\partial \phi_i^m(r_o,z_o)}{\partial z_o} \tag{96}$$

in which α = angle shown in Fig. 2 of $\vec{n}_o$ relative to the horizontal plane such that $\vec{n}_o = (-\cos\alpha, 0, \sin\alpha)$ in terms of the cylindrical coordinate system and $\phi_i^m(r_o,z_o)$ results from the Fourier series expression of ϕ_i in the form of Eq. 90

$$\phi_i^m(r_o,z_o) = \frac{igH}{2\omega} \frac{\cosh k(z_o+d)}{\cosh kd}(-i)^m J_m(kr_o) \tag{97}$$

where g = gravitational acceleration, k = incident wave number and J_m = Bessel function of the first kind of order m (Abramowitz et al., 1972).

In order to find $\phi_j^m(r_o,z_o)$ on L_B, the point (r,z) in Eq. 92 is taken to be on L_B and the resulting equation with $\epsilon = 1/2$ is solved numerically by discretizing L_B into a finite number, N, of short straight segments and assuming that $\phi_j^m(r_o,z_o)$ is constant over each segment and represented by the value at the center of each segment as illustrated in Fig. 2 (Eatock Taylor et al. 1978). The above discretization reduces Eq. 92 to the matrix equation from which the values of $\phi_j^m(r_o,z_o)$ at the center of each segment can be obtained. The details of the numerical computation including the treatment of singularities and discontinuities were given by previous investigators (Eatock Taylor et al., 1978; Fenton, 1978; Isaacson, 1982). Because of Eqs. 93-95, the non-zero values of $\phi_j^m(r_o,z_o)$ associated with the surge (j=1), heave (j=2) and pitch (j=3) motions are $\phi_1^1(r_o,z_o)$, $\phi_2^0(r_o,z_o)$ and $\phi_3^1(r_o,z_o)$ only. Then, Eq. 92 with the point (r,z) taken in the fluid domain, that is, $\epsilon = 1$ indicates that only $\phi_1^1(r,z)$, $\phi_2^0(r,z)$ and $\phi_3^1(r,z)$ for j=1,2 and 3 are non-zero. Consequently, Eq. 90 for j=1,2 and 3 can be simplified as

$$\phi_1(\vec{x}) = 2\phi_1^1(r,z)\cos\theta \quad , \quad \phi_2(\vec{x}) = \phi_2^0(r,z)$$
$$\phi_3(\vec{x}) = 2\phi_3^1(r,z)\cos\theta \tag{98}$$

On the other hand, for the scattered wave (j=4=s) Eq. 92 together with Eqs. 96 and 97 needs to be solved to obtain $\phi_s^m(r_o,z_o)$ and then $\phi_s^m(r,z)$ for m=0,1,2,..., (M-1) in which M is the number of harmonics retained in Eq. 90 such that the contribution of the omitted harmonics is negligible in comparison to that of the retained harmonics. It should also be mentioned that ϕ_s^m is proportional to the wave height H since ϕ_i^m in Eq. 97 is proportional to H. As a result, it is sufficient to solve Eq. 92 with j=4=s for unit wave height and obtain the value of ϕ_s^m divided by H.

The complex amplitudes ξ_j (j=1,2 and 3) associated with the surge, heave and pitch motions of a freely floating axisymmetric body may be found by solving the following equations for n=1,2 and 3 (Isaacson, 1982)

$$\sum_{j=1}^{3} [-\omega^2(M_{nj} + a_{nj}) + i\omega b_{nj} + C_{nj}] \frac{\xi_j}{H} = \frac{F_n}{H} \quad (n=1,2,3) \tag{99}$$

in which M_{nj} = mass matrix components, C_{nj} = hydrostatic stiffness matrix components, a_{nj} = added mass matrix components, b_{nj} = radiation damping matrix components and F_n = exciting force components. M_{nj} and C_{nj} can be computed for a specified body (Isaacson, 1982; Mei, 1983). a_{nj} and b_{nj} are associated with the radiated waves and can be obtained using the computed values of $\phi_1^1(r_o,z_o)$, $\phi_2^0(r_o,z_o)$ and $\phi_3^1(r_o,z_o)$, whereas F_n is caused by the incident and scattered waves and can be found using the known values of $\phi_s^0(r_o,z_o)$, $\phi_s^1(r_o,z_o)$, $\phi_i^0(r_o,z_o)$ and $\phi_i^1(r_o,z_o)$ (Eatock Taylor et al., 1978; Isaacson, 1982). Since F_n and ξ_j are proportional to H, it is sufficient to compute the values of F_n/H and ξ_j/H, that is, the values of F_n and ξ_j for unit wave height

as indicated in Eq. 99.

3.3 Wave Drift Force on a Three-Dimensional Floe

The computation of the mean wave drift force on a freely floating axisymmetric rigid body is made by applying the general formulas presented by Mei (1983) which were originally derived by Maruo (1960) and Newman (1967) using momentum balance. In these formulas, the mean wave drift force and moment are expressed in terms of the scattered and radiated waves in the far field. Alternatively, use may be made of the method based on the direct integration of all pressure contributions upon the instantaneous submerged surface of the body (Pinkster et al., 1983). However, for a single body in regular waves, the momentum approach was found to be more efficient computationally than the direct integration approach (Kokkinowrachos et al., 1983). On the basis of Eq. 90 with j=s for the vertical axisymmetric body, the scattered wave potential in the far field (kr>>1) may be expressed as

$$\phi_s(\vec{x}) = A_s(\theta)\, E(r,z) \qquad \text{for } kr>>1 \tag{100}$$

with

$$A_s(\theta) = A_s^o + 2 \sum_{m=1}^{\infty} A_s^m \cos(m\theta) \tag{101}$$

$$E(r,z) = \frac{igH}{2\omega} \frac{\cosh k(z+d)}{\cosh kd} \left(\frac{2}{\pi kr} \right)^{1/2} \exp\left[-i\left(kr - \frac{\pi}{4} \right) \right] \tag{102}$$

in which $A_s(\theta)$ is the normalized scattered wave amplitude in the far field in the direction θ. The incident wave propagates in the direction $\theta = 0$. The dimensionless complex constants A_s^m (m=0,1,2...) in Eq. 101 are related to $\phi_s^m(r,z)$ by $\phi_s^m = A_s^m E$ in the far field. For kr>>1, Eq. 92 with j=s may be shown to reduce to

$$A_s^m = -\frac{2\pi\omega\ \mathrm{coshkd}}{g}\ \frac{\sigma^2 - k^2}{(k^2-\sigma^2)d+\sigma}\ i^m \int_{L_B}\left\{ \frac{\phi_s^m(r_o,z_o)}{H}\ \frac{\partial}{\partial n_o}\right.$$

$$[\mathrm{coshk}(z_o+d)J_m(kr_o)] - \mathrm{coshk}(z_o+d)J_m(kr_o)\ \frac{\partial}{\partial n_o} \tag{103}$$

$$\left.\left[\frac{\phi_s^m(r_o,z_o)}{H}\right]\right\} r_o dL_B$$

in which $\sigma = \omega^2/g$ and A_s^m is independent of H since the computed values of $\phi_s^m(r_o,z_o)/H$ are independent of H. A_s^m is computed by integrating Eq. 103 numerically along L_B which has been discretized into N short segments.

On the other hand, Eq. 98 indicates that the radiated wave potentials in the far field may be expressed as

$$\phi_1(\vec{x}) = A_1^1 H^{-1}E(r,z)\cos\theta, \qquad \phi_2(\vec{x}) = A_2^o H^{-1}E(r,z),$$

$$\phi_3(\vec{x}) = A_3^1 H^{-1}E(r,z)\cos\theta \qquad \text{for } kr\gg 1 \tag{104}$$

in which A_1^1, A_2^o and A_3^1 are dimensionless complex constants and could be obtained from the far-field asymptotic forms of $\phi_1^1(r,z)$, $\phi_2^o(r,z)$ and $\phi_3^1(r,z)$ in the same way as A_s^m given by Eq. 103. However, it is more efficient to use Haskind-Hanaoka theorem which relates the n-th component of the exciting force to the n-th radiated wave potential for the same body (Mei, 1983). This theorem may be shown to yield the following relationships in the present notation

$$A_1^1 = B\frac{F_1}{H}, \qquad A_2^o = -B\frac{F_2}{H}, \qquad A_3^1 = B\frac{F_3}{H} \tag{105}$$

with

$$B = 2ik^2\left[\rho g\left(1 + \frac{2kd}{\sinh 2kd}\right)\right]^{-1} \tag{106}$$

in which ρ = fluid density and A_1^1, A_2^o and A_3^1 are independent of H.

Moreover, Eqs. 88, 100 and 104 imply that the sum of the scattered and radiated waves in the far field may be expressed as

$$\phi_s(\vec{x}) + \sum_{j=1}^{3} \xi_j \phi_j(\vec{x}) = A(\theta)\, E(r,z) \qquad \text{for } kr \gg 1 \tag{107}$$

with

$$A(\theta) = A_s(\theta) + \frac{\xi_2}{H} A_2^o + \left(\frac{\xi_1}{H} A_1^1 + \frac{\xi_3}{H} A_3^1 \right) \cos\theta \tag{108}$$

in which $A_s(\theta)$ is given by Eq. 101 and $A(\theta)$ is the normalized amplitude in the far field. Eqs. 101 and 108 indicate that $A_s(\theta)$ and $A(\theta)$are symmetric about the axis of θ=0, that is, $A_s(\theta) = A_s(-\theta)$ and $A(\theta) = A(-\theta)$. As a result, it is sufficient to consider the range $0 \le \theta \le \pi$.

Finally, applying the formulas presented by Mei (1983), the wave drift force in the x-direction, F_d, for the vertical axisymmetric body is computed from

$$f_d = \frac{F_d}{\rho g H^2 D} = -\,(4kD)^{-1} \left(1 + \frac{2kd}{\sinh 2kd} \right) \left\{ \frac{1}{\pi} \int_0^{\pi} \cos\theta \, |A(\theta)|^2 d\theta + R_e[A(0)] \right\} \tag{109}$$

in which D = characteristic horizontal length of the body and f_d = normalized wave drift force which is independent of H. It should be noted that for the vertical axisymmetric body the mean drift force acts only in the direction of wave propagation, that is, in the x-direction. Furthermore, the mean second-order drift force depends on the first-order quantities only (Mei, 1983; Pinkster et al., 1983).

One way to check the accuracy of the computation of f_d by use of Eq. 109

is to examine whether the computed values of $A_s(\theta)$ and $A(\theta)$ satisfy the energy conservation relationships for $A_s(\theta)$ and $A(\theta)$ presented by Mei (1983) which for the vertical axisymmetric body can be written as

$$\frac{1}{\pi}\int_0^{\pi} |A_s(\theta)|^2 d\theta = - R_e[A_s(0)] \tag{110}$$

$$\frac{1}{\pi}\int_0^{\pi} |A(\theta)|^2 d\theta = - R_e [A(0)] \tag{111}$$

Eq. 111 is valid as long as the freely oscillating body does not absorb or dissipate the wave energy. Eqs. 110 and 111 are used herein to check the accuracy of the computation of f_d using Eq. 109.

Furthermore, the computed values of A_s^m using Eq. 103 may be compared with the analytical solution for a fixed vertical cylinder of diameter D (e.g., Mei, 1983). For this case, A_s^m can be shown to be given by

$$A_s^m = - J_m'(\beta)[J_m'(\beta) - i\, Y_m'(\beta)]^{-1} \quad (m=0,1,2,\ldots) \tag{112}$$

in which Y_m = Bessel function of the second kind of order m (Abramowitz et al., 1972) and the prime indicates the differentiation with respect to $\beta = (\pi D/L)$ with D = diameter of the cylinder and L = wavelength.

3.4 Accuracy of Numerical Method

A computer program was developed by Kobayashi et al. (1986, 1987) to compute the wave drift force on a vertical axisymmetric ice floe using Eq. 109. The normalized far-field wave amplitude $A(\theta)$ in Eq. 109 is defined by Eq. 108 and includes the complex amplitudes ξ_j (j=1,2 and 3) for the surge, heave and pitch motions as well as the exciting force components F_n (n=1,2 and

3) due to the incident and scattered waves. As a first step for insuring the accuracy of the developed computer program, the computed values of ξ_j and F_n were compared with available analytical and numerical solutions in the same way as Eatock Taylor et al. (1978) and Isaacson (1982). The compared results presented by Frankenstein (1986) indicated the accuracy of the developed program for computing ξ_j and F_n. The number of segments, N, used to approximate the body contour L_B was taken to be N = 30 in the computation although a smaller value of N could be sufficient. The use of N=30 was possible since the computational procedure is highly efficient. The length of each segment was taken to be equal except for waves of small period for which more segments were required near the free surface since the wave action is essentially limited to the region $z \gtrsim (-L/2)$ where L = wavelength.

In addition, comparison was made with the small-scale model tests of Lever et al. (1984) who measured the motions of spherical, cubical and rectangular prismatic ice models made of paraffin wax. The compared results were presented by Kobayashi et al. (1986) who approximated the cubes and rectangular prisms by the corresponding vertical axisymmetric cylinders of the same height and mass. The agreement between the linear analysis and the measured ice motions was found to be only qualitative probably because of the measurement uncertainties and the limitations of the linear potential theory for predicting the resonant amplitude of the heave motion of an ice floe. The maximum translational velocities computed by Kobayashi et al. (1986) indicated large values during severe storms.

As for the wave drift force computation using Eq. 109 with $A(\theta)$ given by Eq. 108, it is required to ascertain the accuracy of the computation of $A_s(\theta)$

which is defined by Eq. 101 with A_s^m computed using Eq. 103. For the computation the infinity of the summation in Eq. 101 is replaced by (M-1) where M is the number of harmonics included in the computation. In order to estimate an appropriate value of M required for the computation, the normalized wave drift force, f_d, for a fixed vertical cylinder of diameter D was calculated by Kobayashi et al. (1987) using the analytical solution for which A_s^m is given by Eq. 112. The calculated values of f_d were plotted as a function of the wave period T for the cylinder of D = 20 m in the water depth d = 100 m which was essentially deep water for $T \leq 11$ sec. M=8 was found to be sufficient for $T \geq 2.7$ sec ($L/D \geq 0.57$) and reasonable for $T \geq 2.1$ sec ($L/D \geq 0.34$) where Isaacson (1982) indicated that M=8 would be sufficient for computing the circumferential variation of wave runup around the cylinder. However, the value of M greater than 80 or so was needed in the range T = 1-2 sec. Consequently, a large number of harmonics were required to describe the circumferential variation of $A_s(\theta)$ around a large body for which the value of L/D was small. Extrapolation of the computed results to the limit $T \to 0$ appeared to suggest that $f_d \simeq 1/12$ as $L/D \to 0$. Comparison was also made of the numerical and analytical variations of $|A_s(\theta)|^2$ with respect to θ for T=5 and 8 sec where use was made of D=20 m, d=100 m and M=8. $|A_s(\theta)|^2$ indicates the circumferential variation of the scattered wave energy in the far field. The numerical results based on Eq. 103 were found to be in good agreement with the analytical results based on Eq. 112. The scattered wave energy in the far field was concentrated near $\theta=0$ and $\theta=\pi/2$ for T = 5 sec (L/D=2.0) and near $\theta = \pi$ for T = 8 sec (L/D=5.0) where the axis of $\theta = 0$ was in the direction of the incident wave propagation. $|A_s(\theta)|^2$ was larger for T = 5 sec than for T = 8 sec. As the wavelength L of the incident wave with given height H became

smaller relative to the diameter D, the scattered wave energy in the far field and the resulting wave drift force on the body normally increased. In summary, the computer program developed by Kobayashi et al. (1986,1987) has been shown to be accurate and efficient except for a very large body relative to the incident wavelength.

4.0 EXAMPLE COMPUTATIONS

In this section, the computed results for the two-dimensional thin elastic ice raft analyzed in Section 2.0 and the vertically axisymmetric rigid ice mass analyzed in Section 3.0 are discussed to gain a physical insight into the mechanism of the wave and ice interaction. The differences and similarity between the elastic and rigid ice floes are examined to assess the sensitivity of the computed results to the assumed characteristics and responses.

4.1 Computed Results for Elastic Ice Floes

The computed results presented in the following are based on the approximate solution for deep water depth and the required computation procedure given in Sections 2.4 and 2.5, respectively. The input parameters required for the computation are taken as

Gravitational acceleration	$g = 9.81$ m/sec^2
Density of the sea water	$\rho = 1025$ kg/m^3
Density of the ice	$\rho_i = 922.5$ kg/m^3
Young's modulus of the elastic ice	$E_i = 6.0 \times 10^9$ N/m^2
Poisson's ratio of the elastic ice	$\nu = 0.3$
Width of the ice raft	D = 10, 30 and 50 m
Thickness of the ice	h = 0.3, 1.0 and 2.0 m
Incident wave period	T = 1 - 10 sec

The typical values of ρ, ρ_i, E_i and ν assumed above are the same as those assumed by Wadhams (1973) and Squire (1984a). The assumed ranges of D, h and T may be typical for the marginal ice zone in the Bering Sea (Squire, 1983b;

Wadhams, 1983; Madsen et al., 1986). For the computation, use is made of T = 1.0, 1.5, 2.0, ..., 10 sec. The water depth d is assumed to be deep. The deep-water assumption should be valid if $d > 0.5\ L$, that is, $d > 78$ m for $T \leq 10$ sec in which $L = (2\pi/k) = (gT^2/2\pi)$ = deep-water wavelength. The incident wave height, H, is not required to be specified since only the normalized quantities are computed herein.

Fig. 3 shows the wavelength $L_1 = (2\pi/K_1)$ in the ice-covered region as a function of the incident wave period T for h = 0.0, 0.3, 1.0 and 2.0 m in which the case of h = 0.0 m corresponds to the open water, that is, $L_1 = L$. It should be noted that the values of K_1, K_2 and K_3 computed from Eq. 55 do not depend on the width D. Fig. 3 indicates that L_1 increases as T and h are increased. Figs. 4-6 show the variations of K_1/k, K_r/k and K_i/k with respect to T for h = 0.3, 1.0 and 2.0 m, respectively, where K_r and K_i are defined in Eq. 71 and determine K_2 and K_3. The wave number K_1 associated with the propagating mode in the ice-covered region approaches the wave number k in the open water as the wave period T is increased. K_r/k and K_i/k tend to increase as T is increased.

On the other hand, the wave reflection coefficient R and the wave transmission coefficient T_r calculated using Eq. 47 as well as the normalized wave drift force f_d defined in Eq. 53 are computed as a function of T = 1.0, 1.5, 2.0, ... , 10 sec with D =10, 30 and 50 m for h = 0.3, 1.0 and 2.0 m. The computed results are plotted in Figs. 7-15 where straight lines are drawn between the computed points. It is obvious that more computed points are required to draw smooth curves in these figures especially for Figs. 7-9 for h = 0.3 m. Figs. 7, 10 and 13 show that R tends to decrease from unity and approach zero with the increase of T although the computed values of R fluctuate. Conversely, Figs. 8, 11 and 14 show that T_r tends to increase from

zero and approach unity with the increase of T since $(R^2 + T_r^2) = 1$ from Eq. 49. On the other hand, $f_d = (R^2/8)$ in deep water from Eq. 53. Consequently, f_d tends to decrease from 1/8 and approach zero rapidly as T is increased. In order to illustrate the effect of h on R, T_r and f_d, the computed values of R, T_r and f_d are plotted as a function of T with h = 0.3, 1.0 and 2.0 m for D = 30 m in Figs. 16, 17 and 18, respectively. Figs. 16 and 18 indicate that the values of R and f_d for given T tend to increase as the thickness of the ice is increased, while Fig. 17 shows the opposite trend for T_r.

Moreover, the normalized amplitude η_m given by Eq. 70 of the vertical displacement of the ice raft located in the region $0 \leq x \leq D$ is plotted as a function of x/D for T = 2, 4, 6 and 8 sec in Figs. 19-27 in which h = 0.3, 1.0 or 2.0 m and D = 10, 30 or 50 m. The value of η_m is the local amplitude normalized by the incident wave amplitude(H/2). Figs. 19-27 show that the values of η_m are typically of the order unity. This implies that the vertical displacement of the ice raft is typically of the same order of magnitude as the vertical displacement of the water particle at the free surface. The variation of η_m with respect to x/D, which is related to the bending moment and shear of the ice raft, tends to decrease as T is increased. This suggests that the ice raft tends to behave like the water particle at the free surface as the width D of the ice raft becomes small relative to the incident wavelength $L = (gT^2/2\pi)$. Accordingly, for the case of $D \ll L$, R and f_d approach zero and T_r approaches unity. On the other hand, $R \simeq 1$, $f_d \simeq 1/8$ and $T_r \simeq 0$ as the ice raft becomes thick and wide relative to the incident wavelength L. In other words, the incident waves tend to be reflected by the thick and wide ice raft which does not move much vertically as may be inferred from the curve for T = 2 sec in Fig. 27. However, most of the computed results shown in this section fall between these two extreme cases.

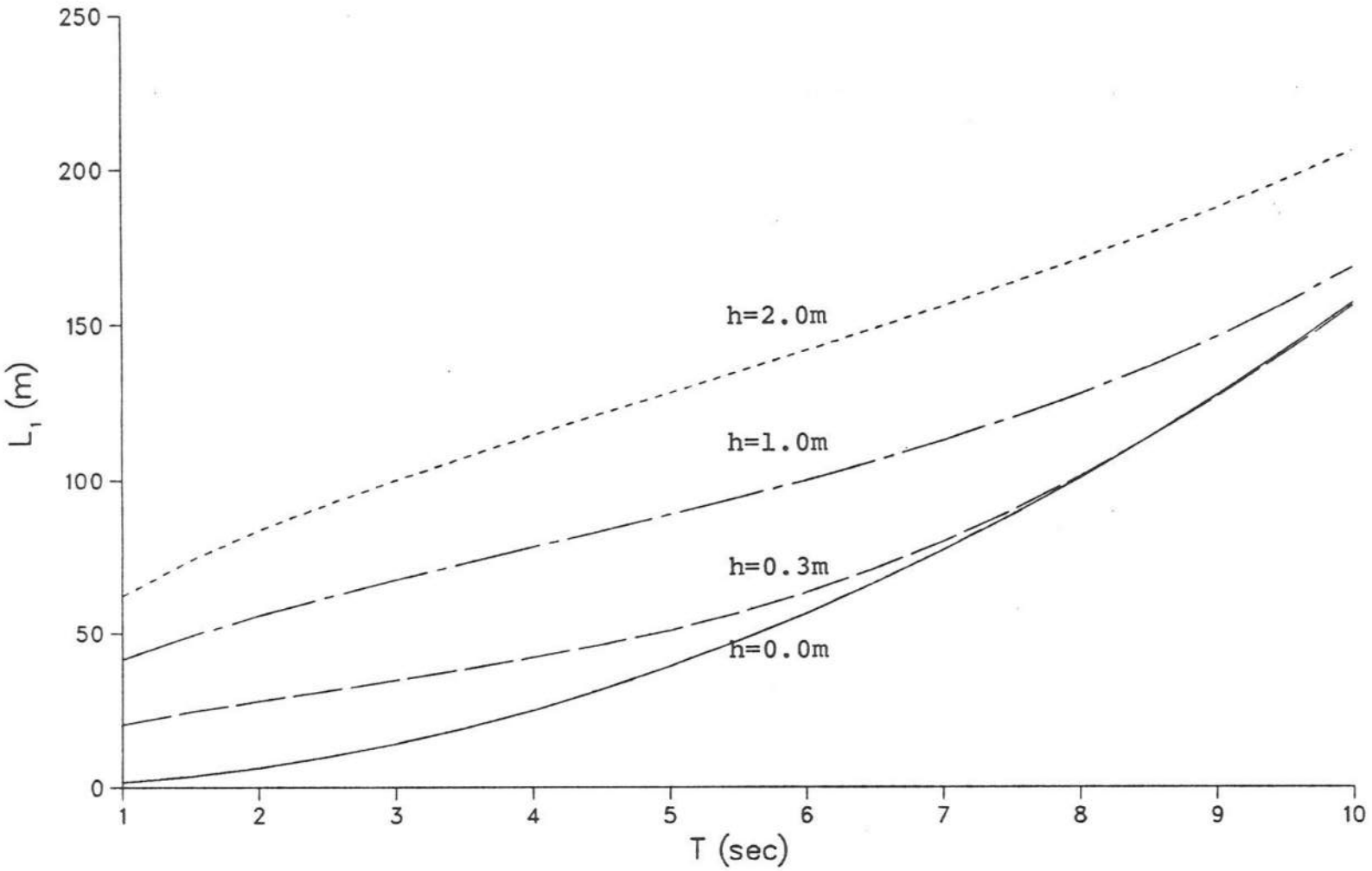

Fig. 3 - Wavelength L_i as a Function of Wave Period T for h = 0.0, 0.3, 1.0 and 2.0 m.

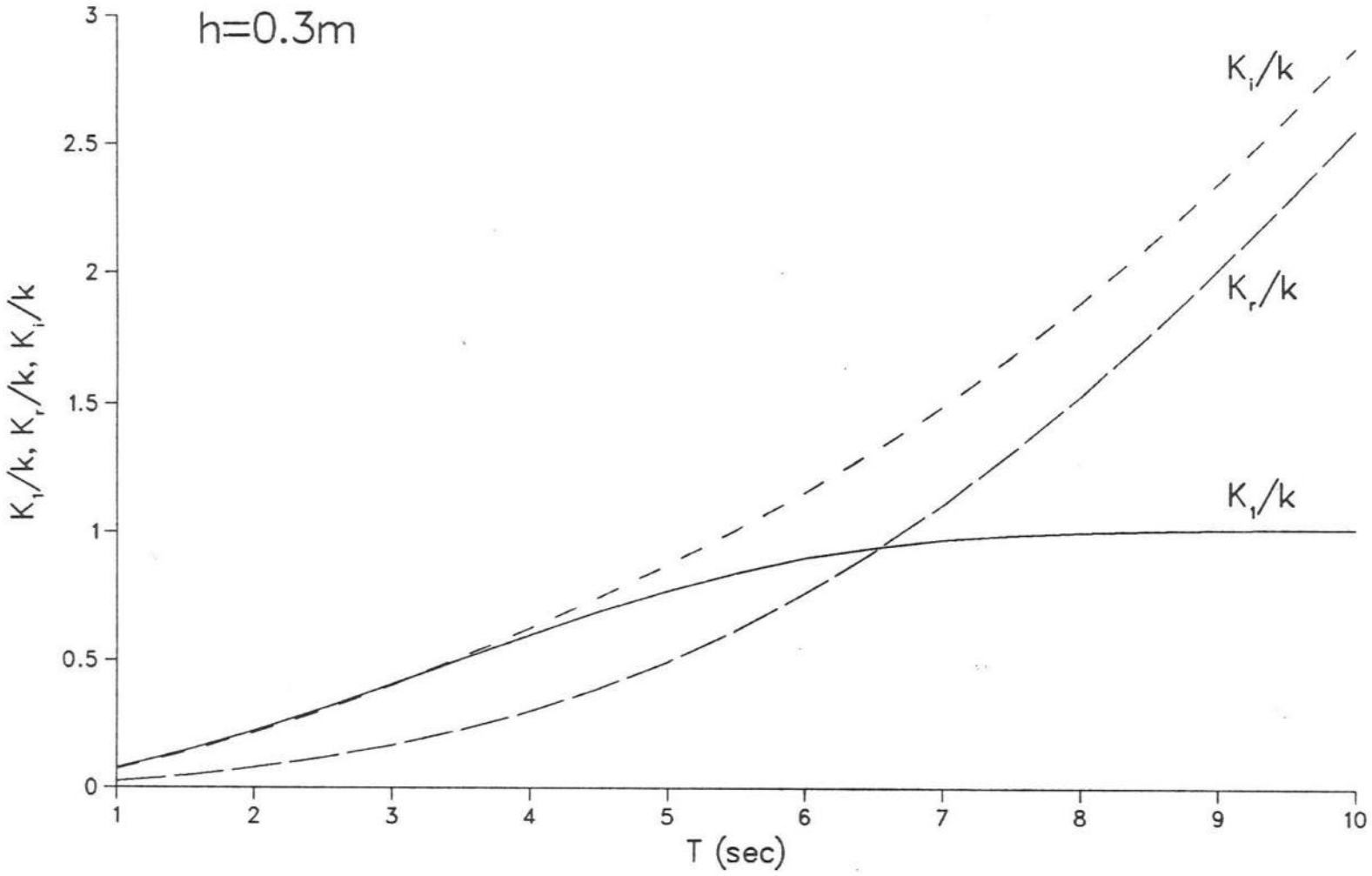

Fig. 4 - K_1/k, K_r/k and K_i/k as a Function of T for h = 0.3 m.

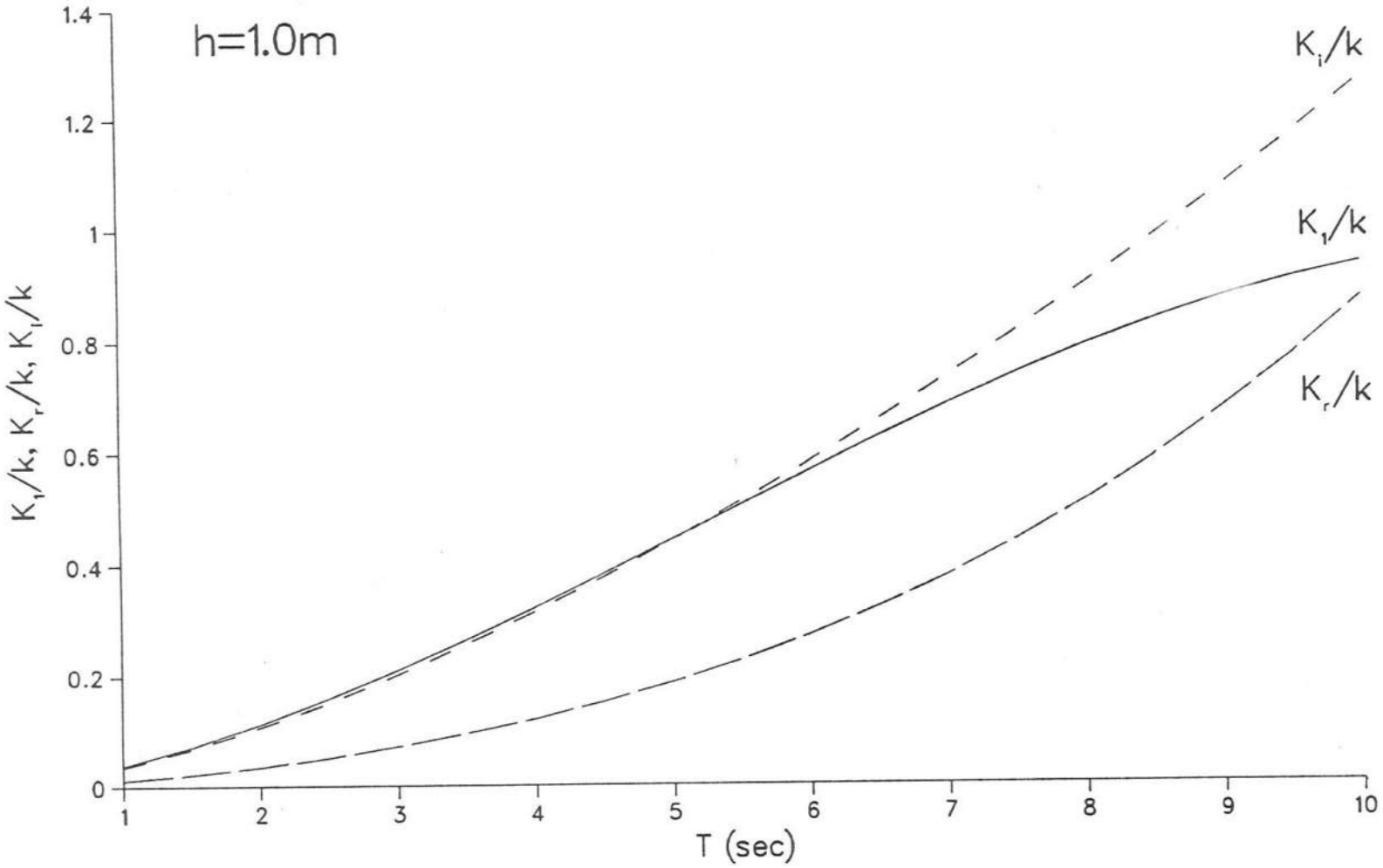

Fig. 5 - K_1/k, K_r/k and K_i/k as a Function of T for h = 1.0 m.

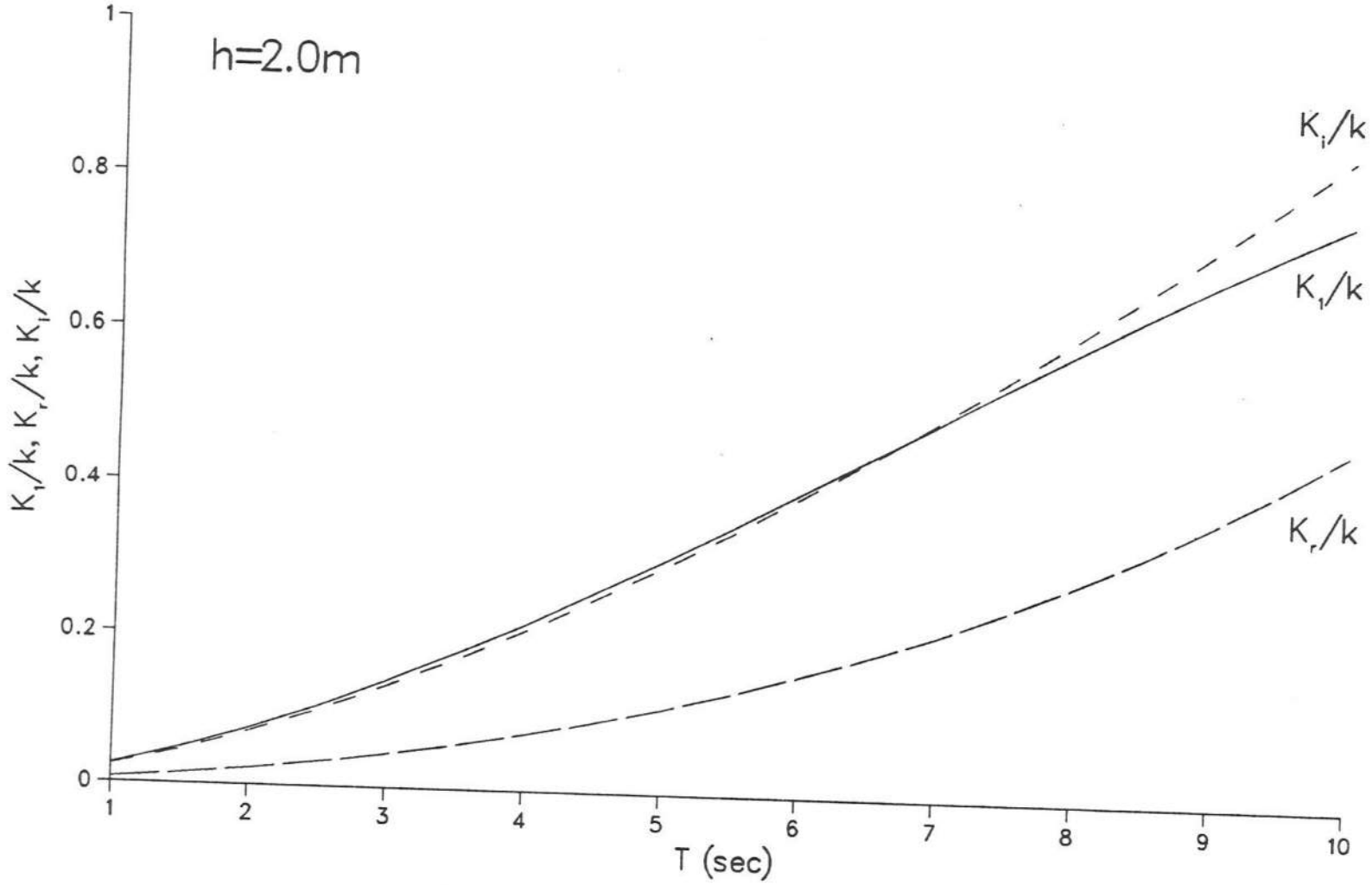

Fig. 6 - K_l/k, K_r/k and K_i/k as a Function of T for h = 2.0 m.

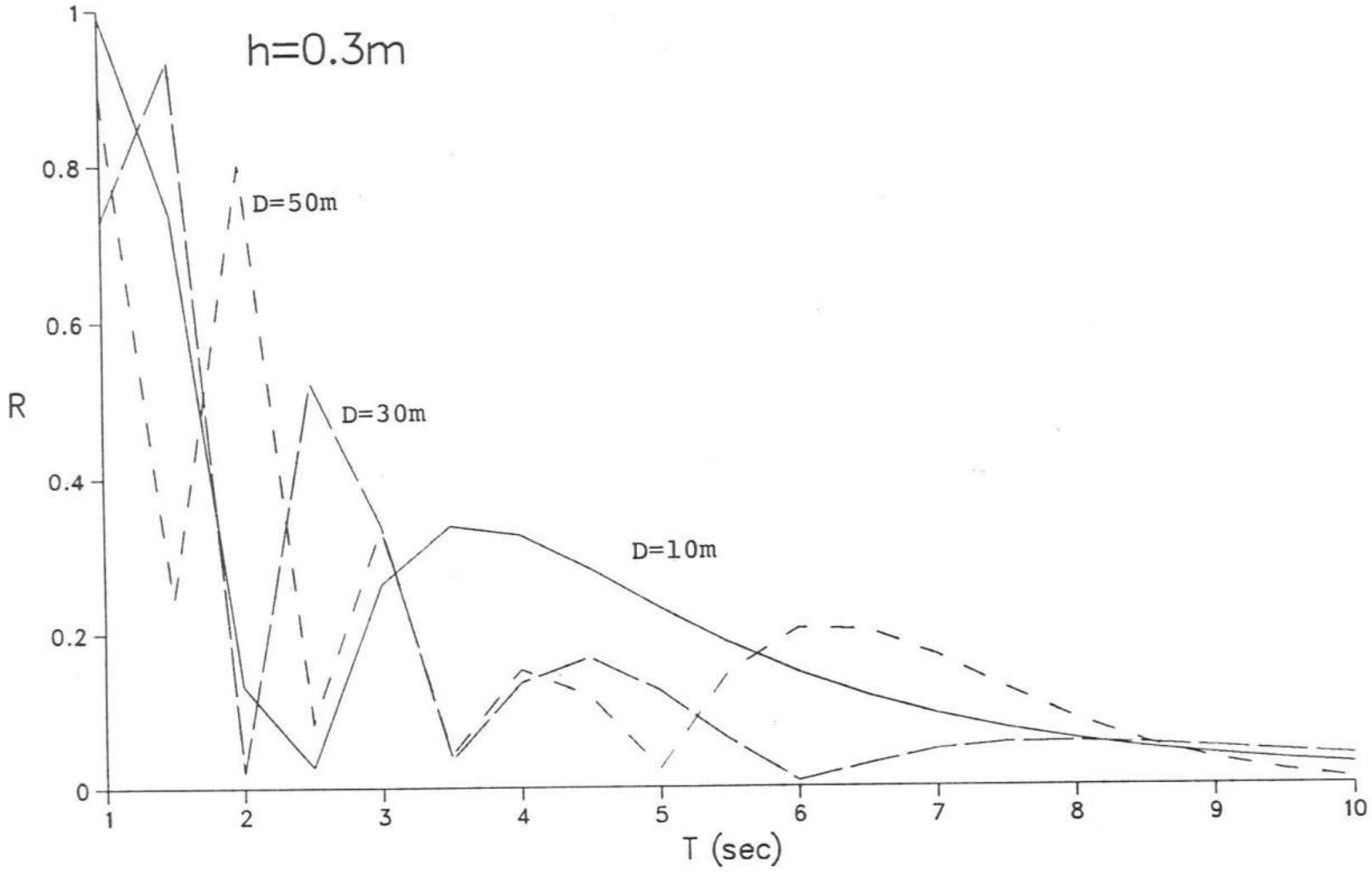

Fig. 7 - R as a Function of T with D = 10, 30 and 50 m for h = 0.3m.

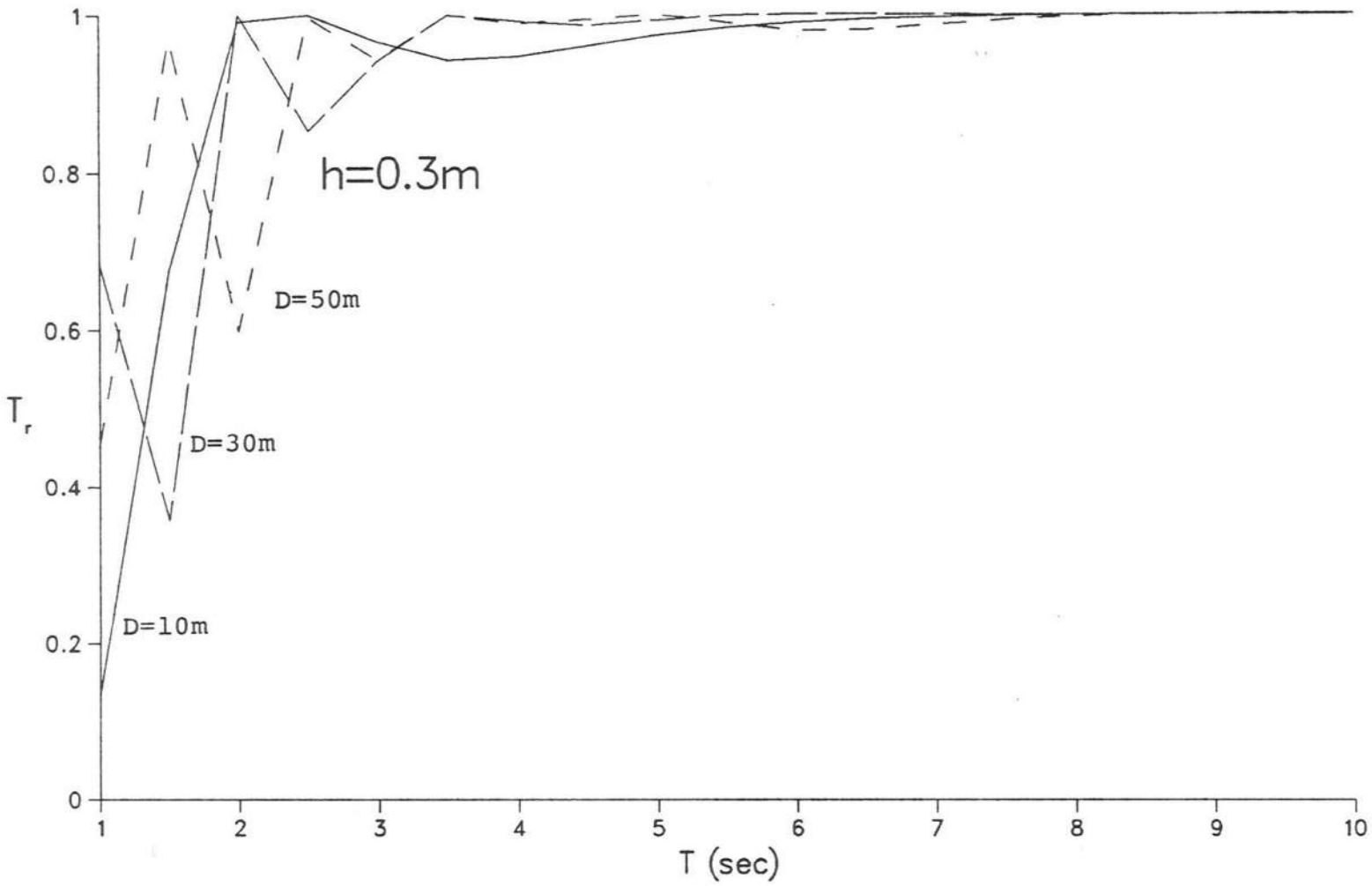

Fig. 8 - T_r as a Function of T with D = 10, 30 and 50m for h = 0.3m.

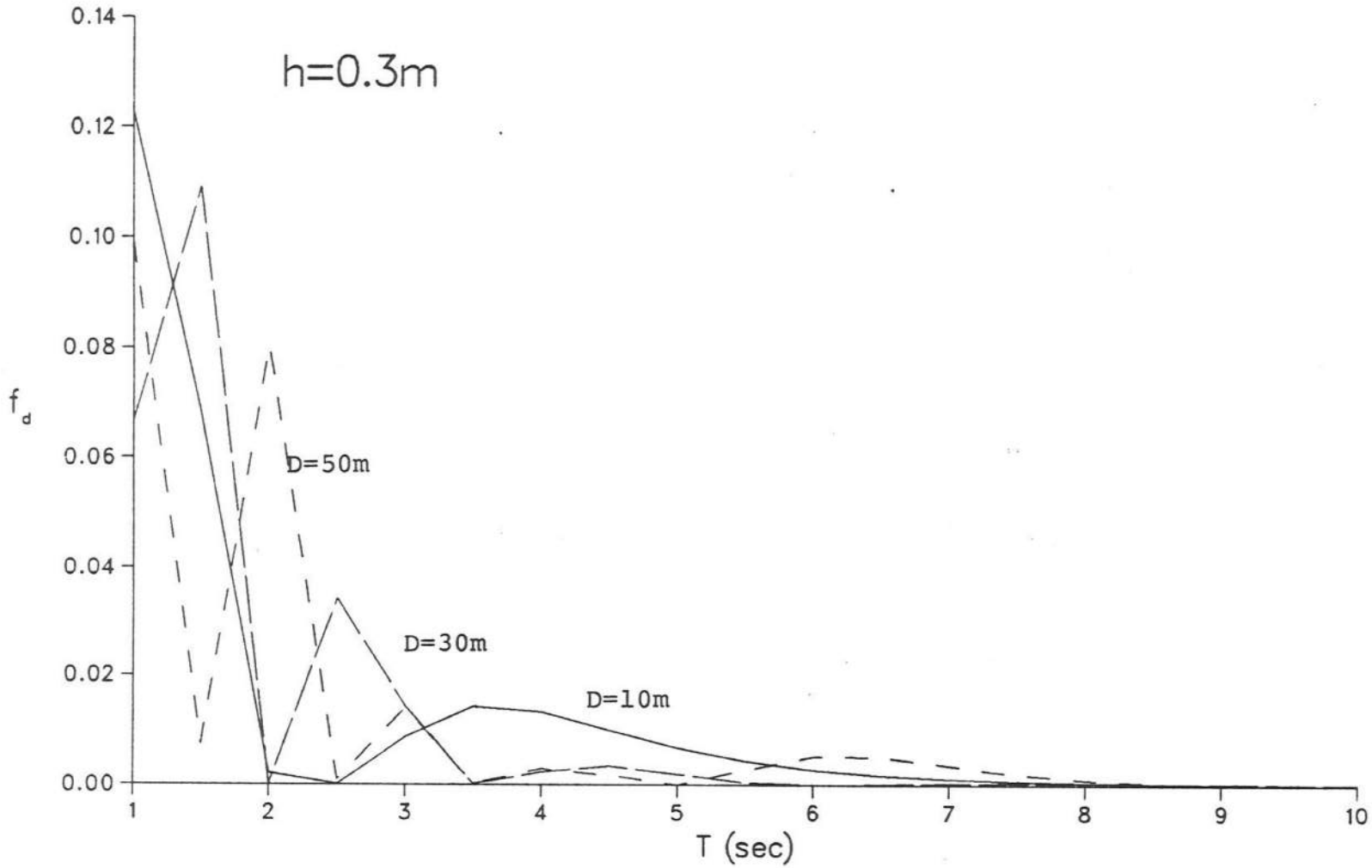

Fig. 9 - f_d as a Function of T with D = 10, 30 and 50m for h = 0.3m.

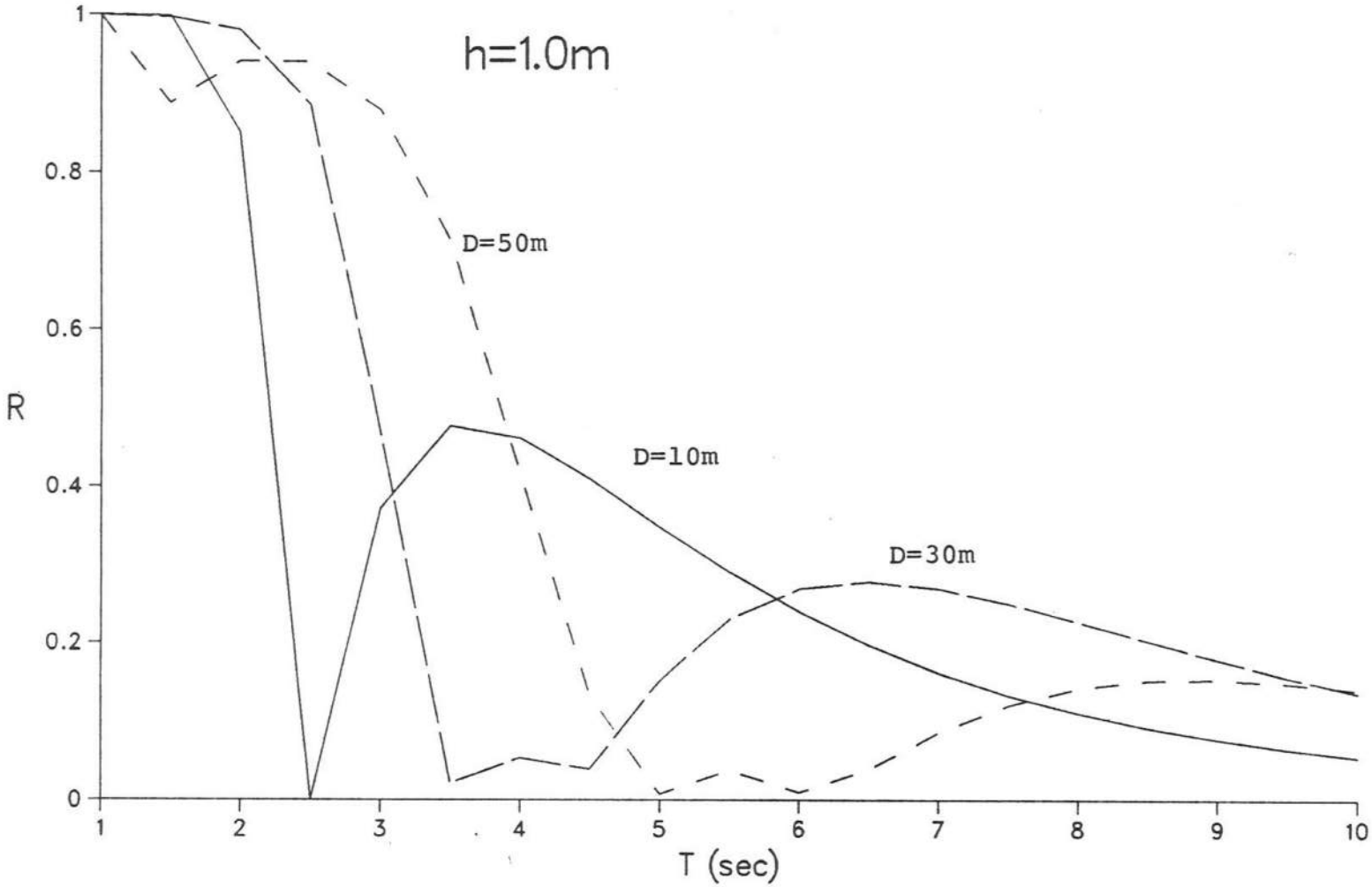

Fig. 10 - R as a Function of T with D = 10, 30 and 50m for h = 1.0m.

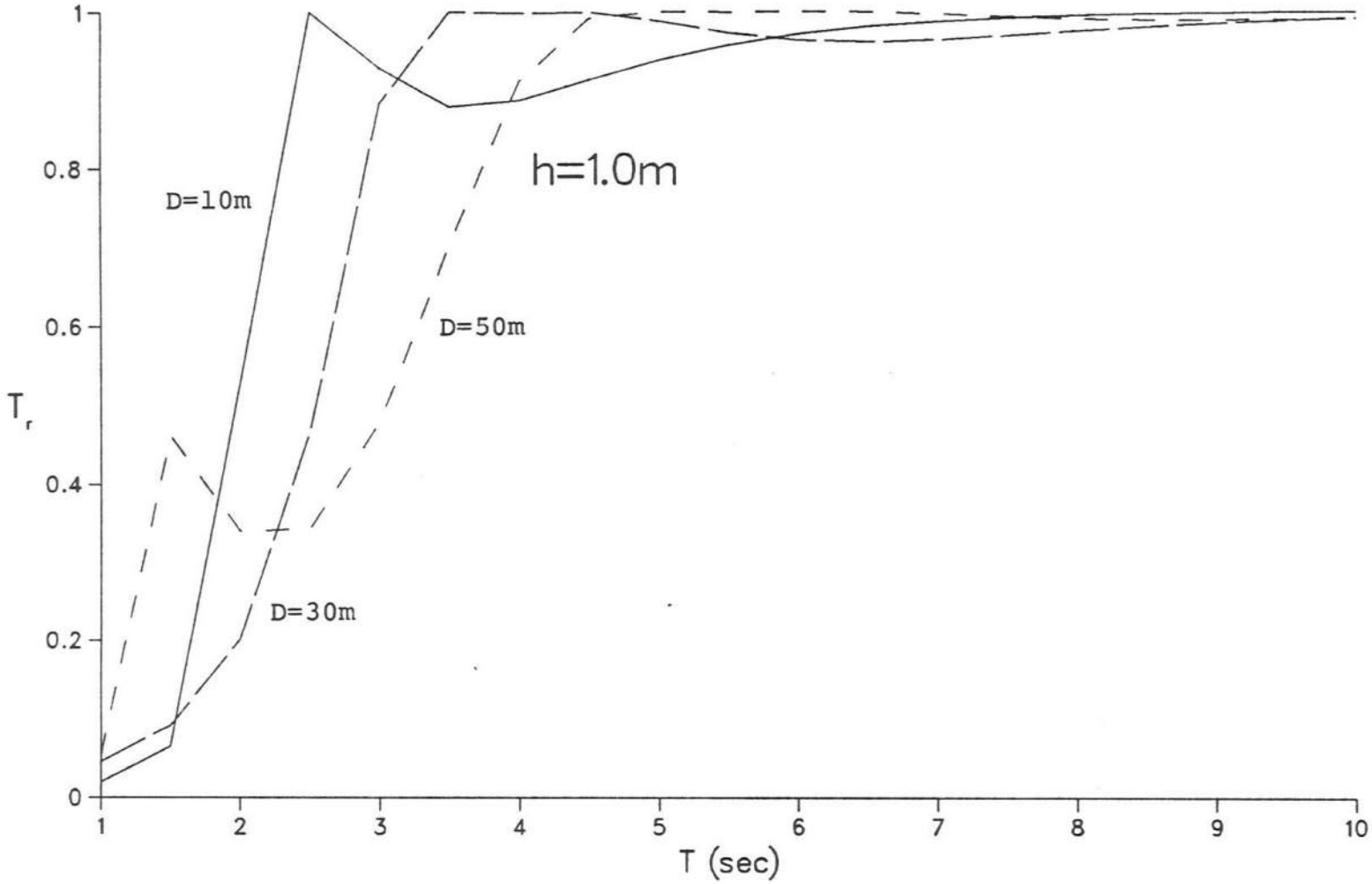

Fig. 11 - T_r as a Function of T with D = 10, 30 and 50m for h = 1.0m.

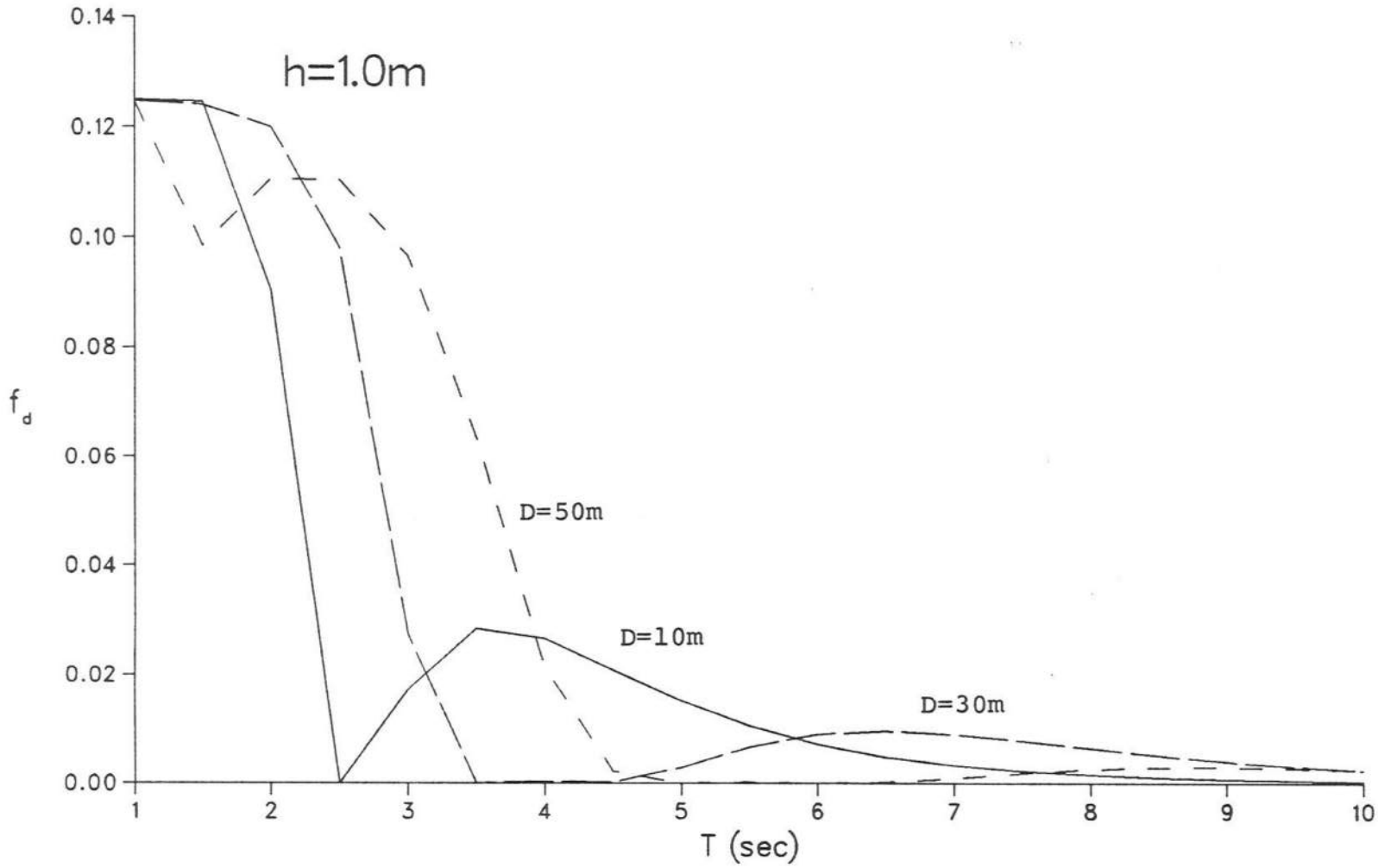

Fig. 12 - f_d as a Function of T with D = 10, 30 and 50m for h = 1.0m.

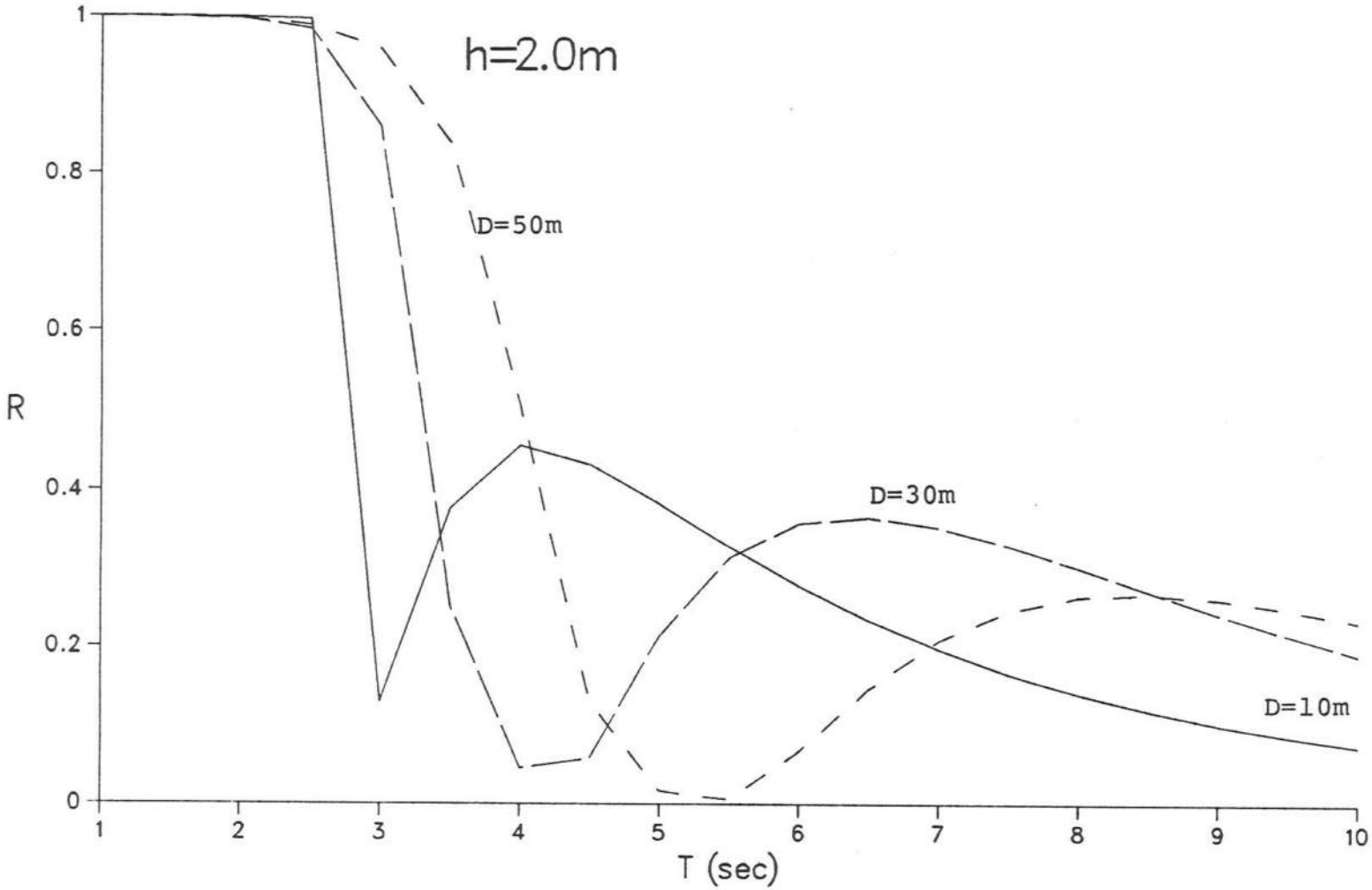

Fig. 13 - R as a Function of T with D = 10, 30 and 50m for h = 2.0m.

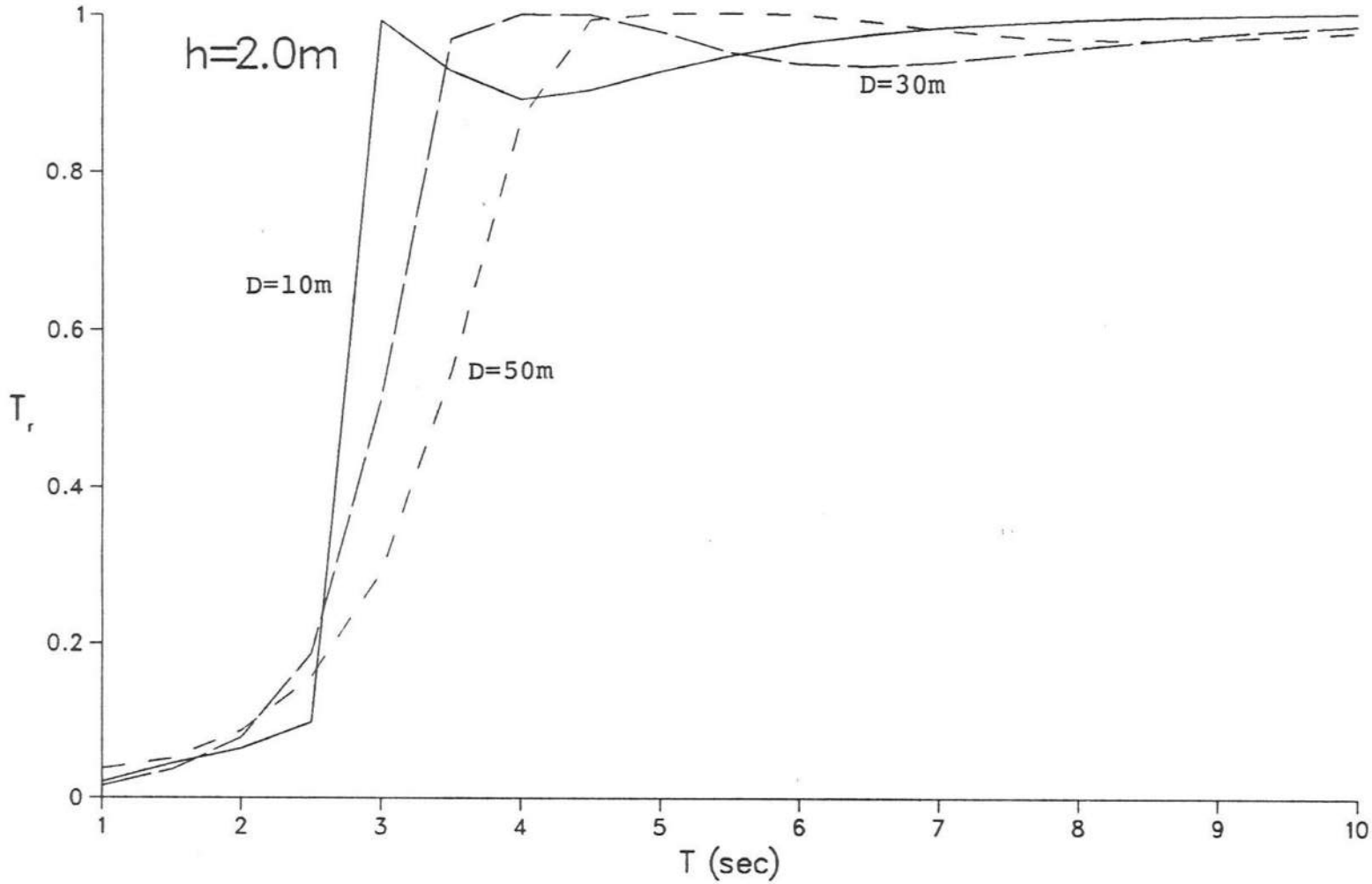

Fig. 14 - T_r as a Function of T with D = 10, 30 and 50m for h = 2.0m.

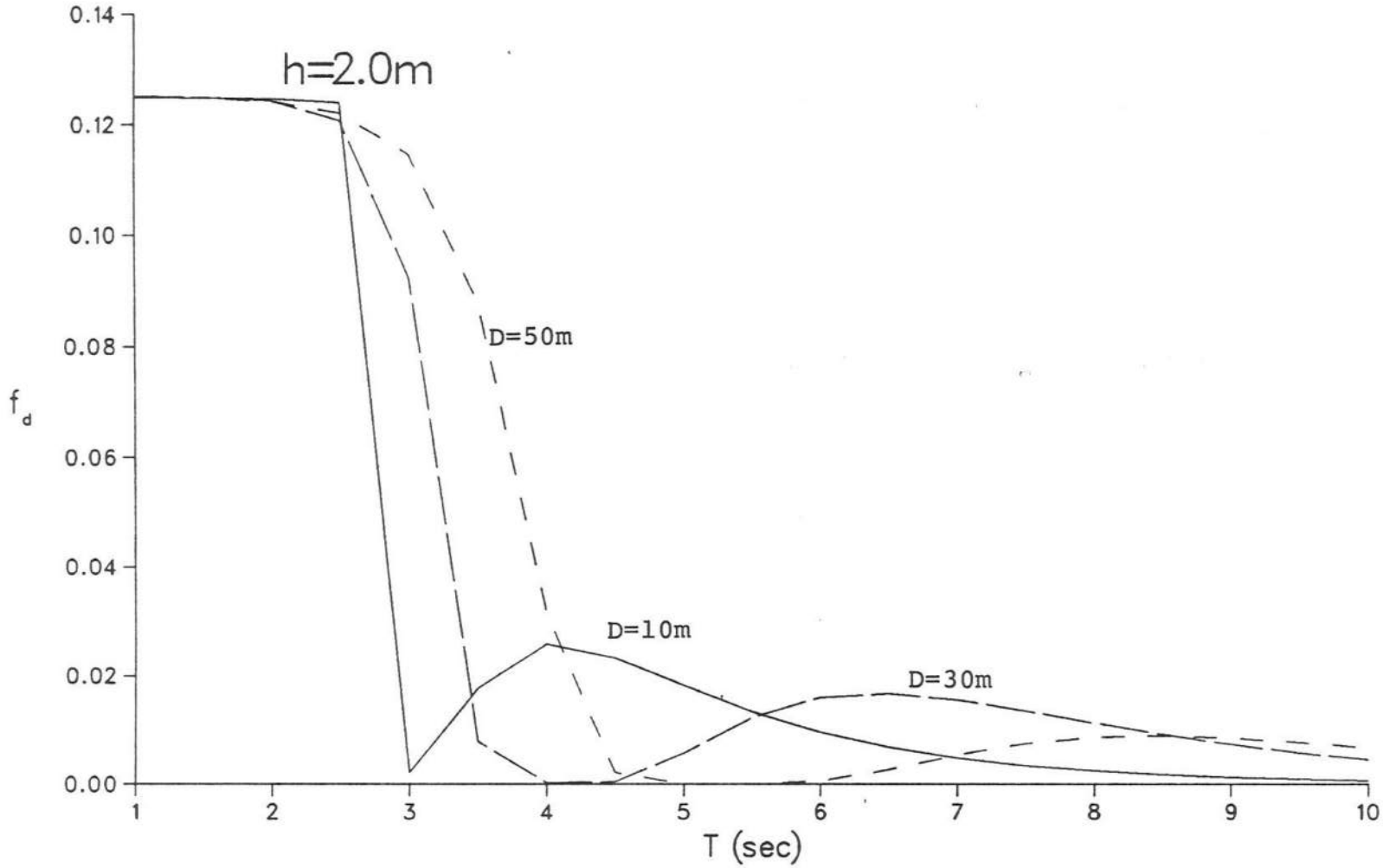

Fig. 15 - f_d as a Function of T with D = 10, 30 and 50m for h = 2.0m.

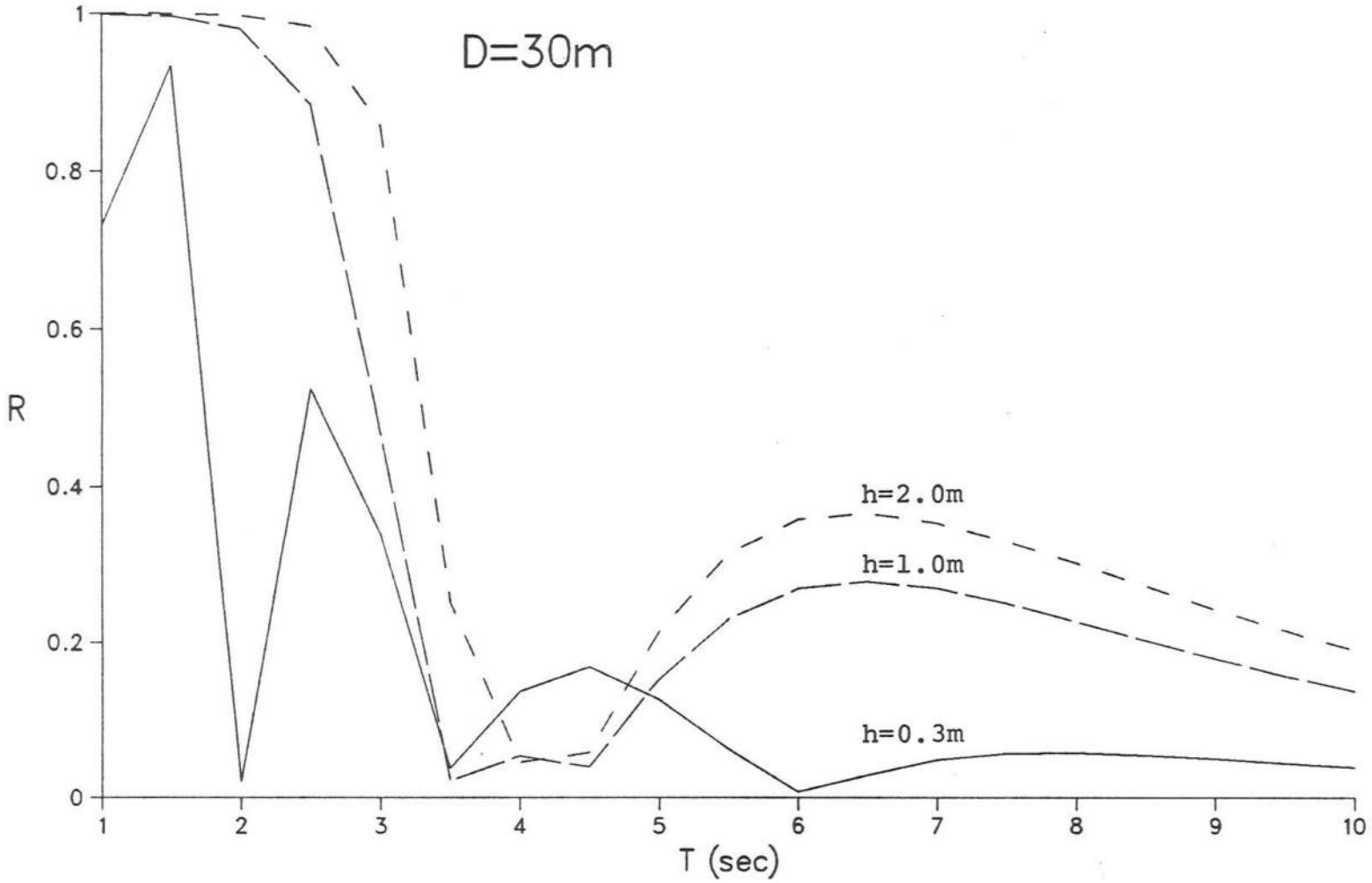

Fig. 16 - R as a Function of T with h = 0.3, 1.0 and 2.0m for D = 30m.

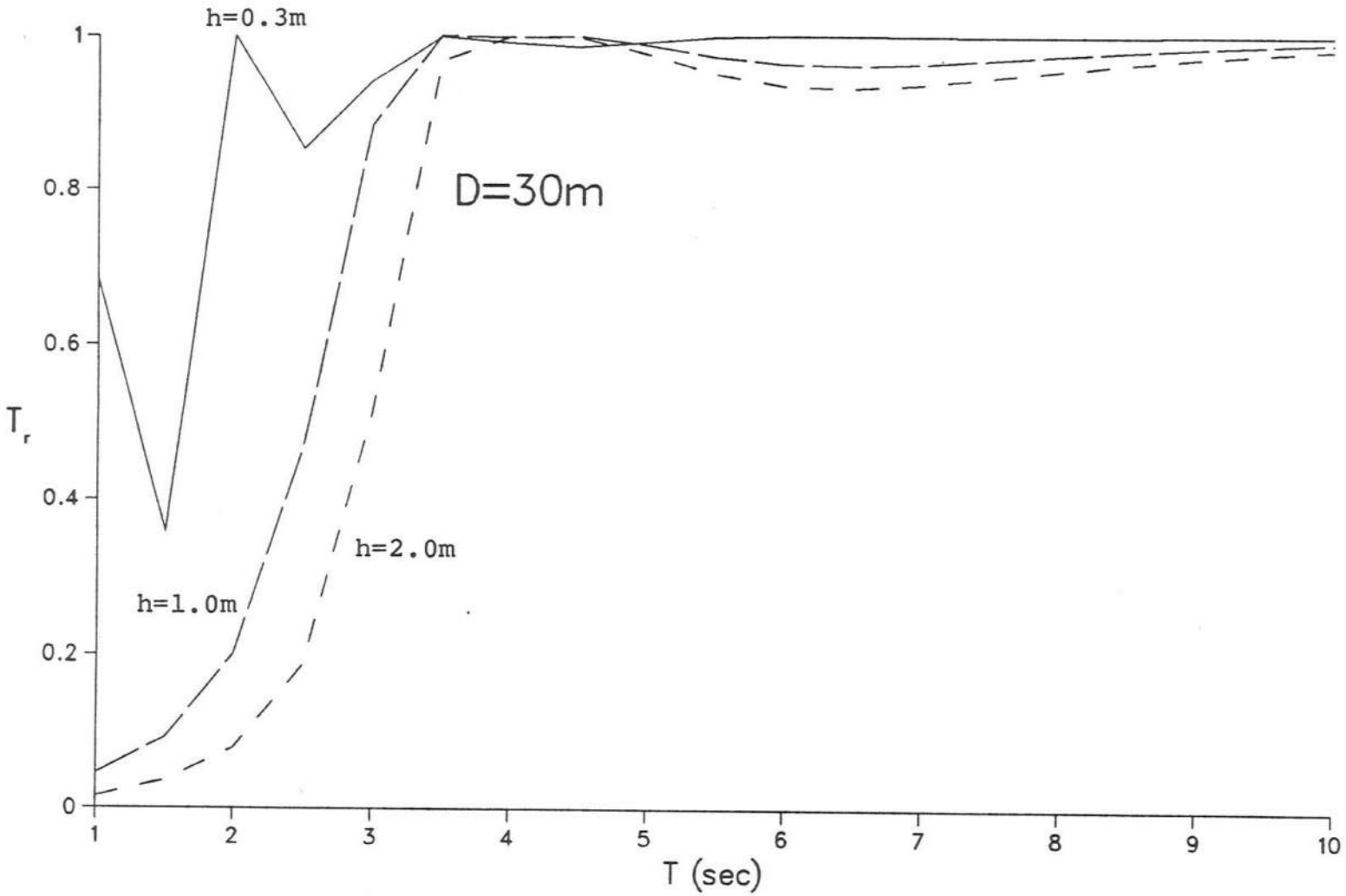

Fig. 17 - T_r as a Function of T with h = 0.3, 1.0 and 2.0m for D = 30m.

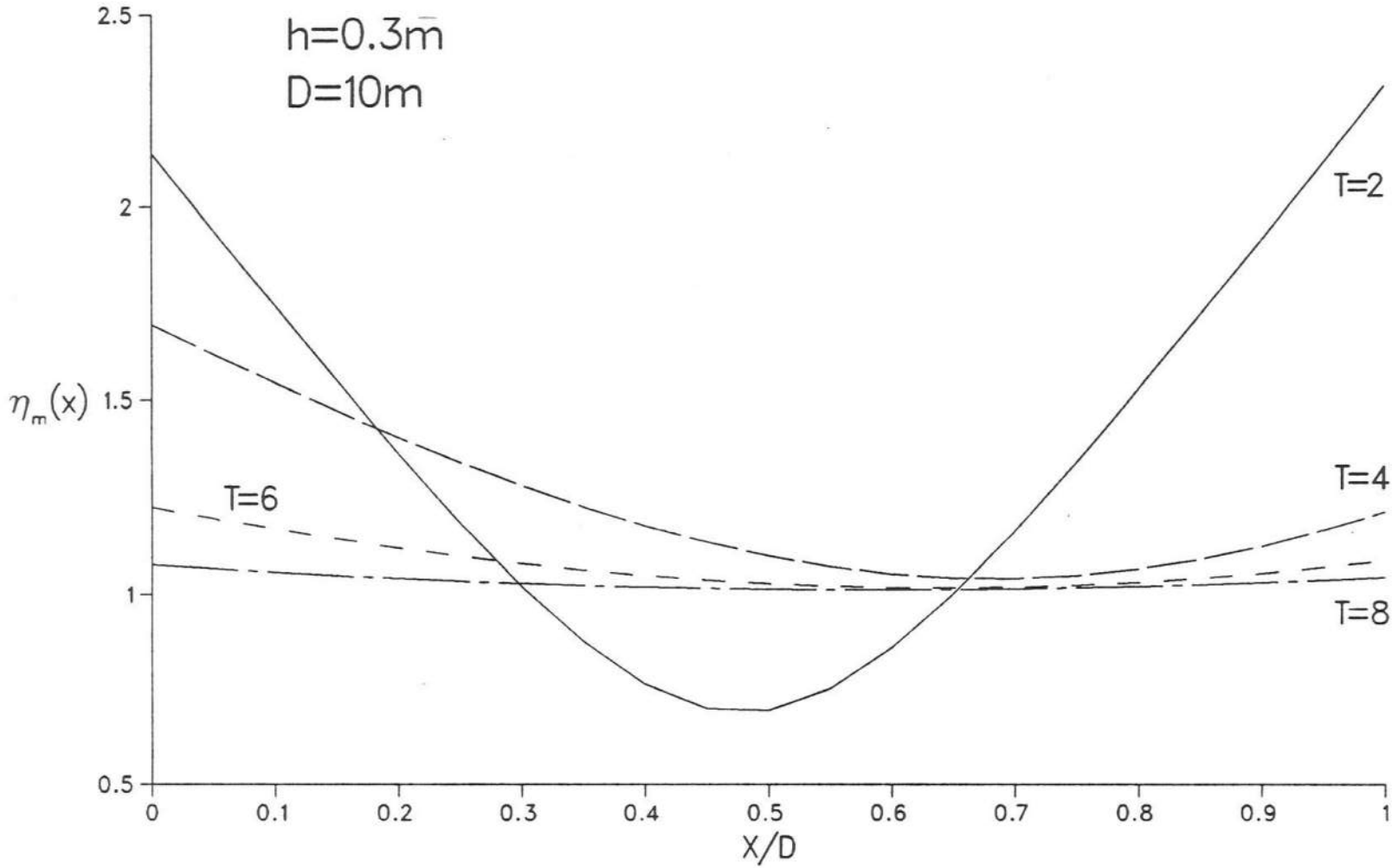

Fig. 19 - η_m as a Function of x/D with T = 2, 4, 6 and 8 sec for h = 0.3m and D = 10m.

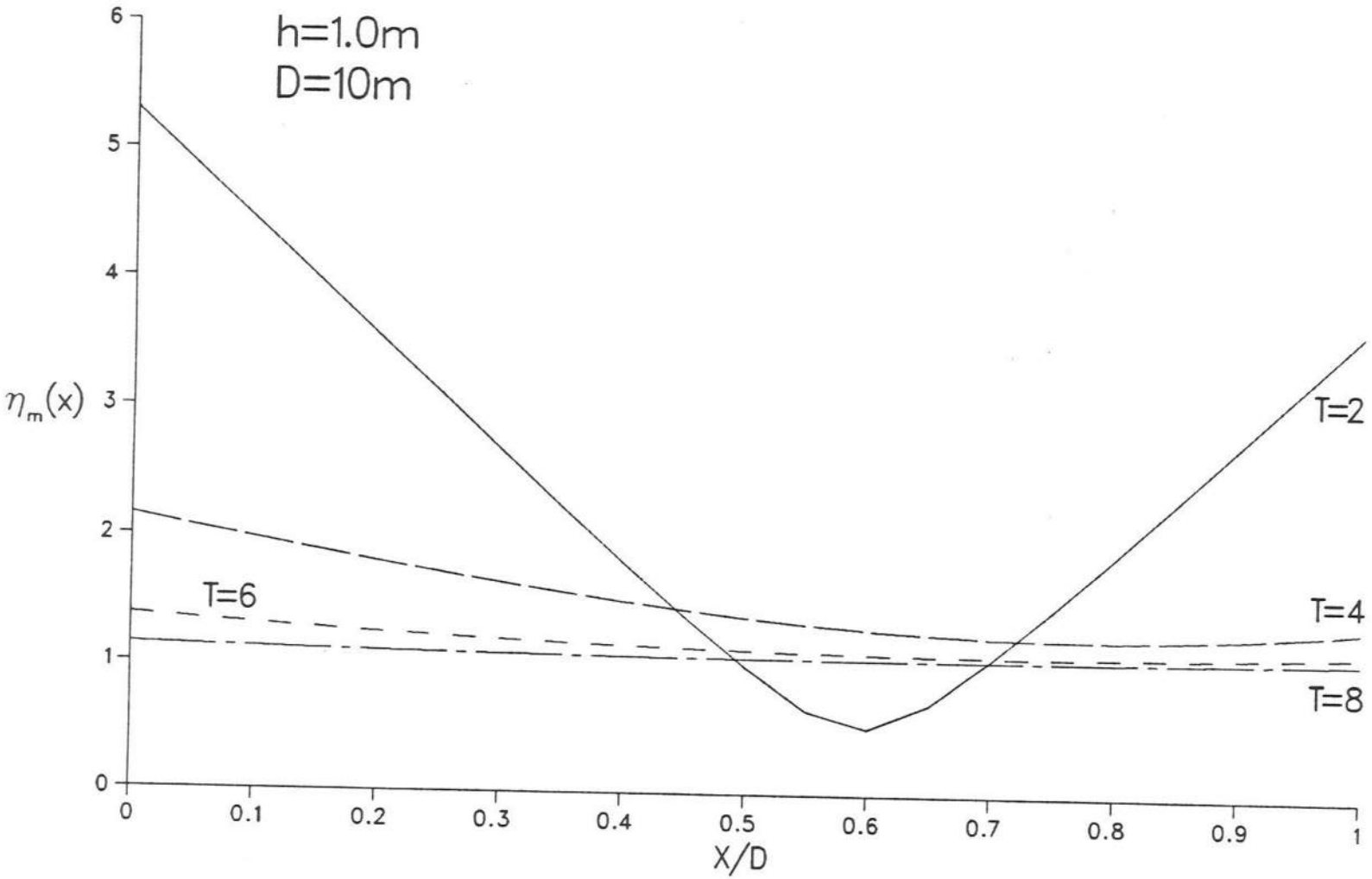

Fig. 20 - η_m as a Function of x/D with T = 2, 4, 6 and 8 sec for h = 1.0m and D = 10m.

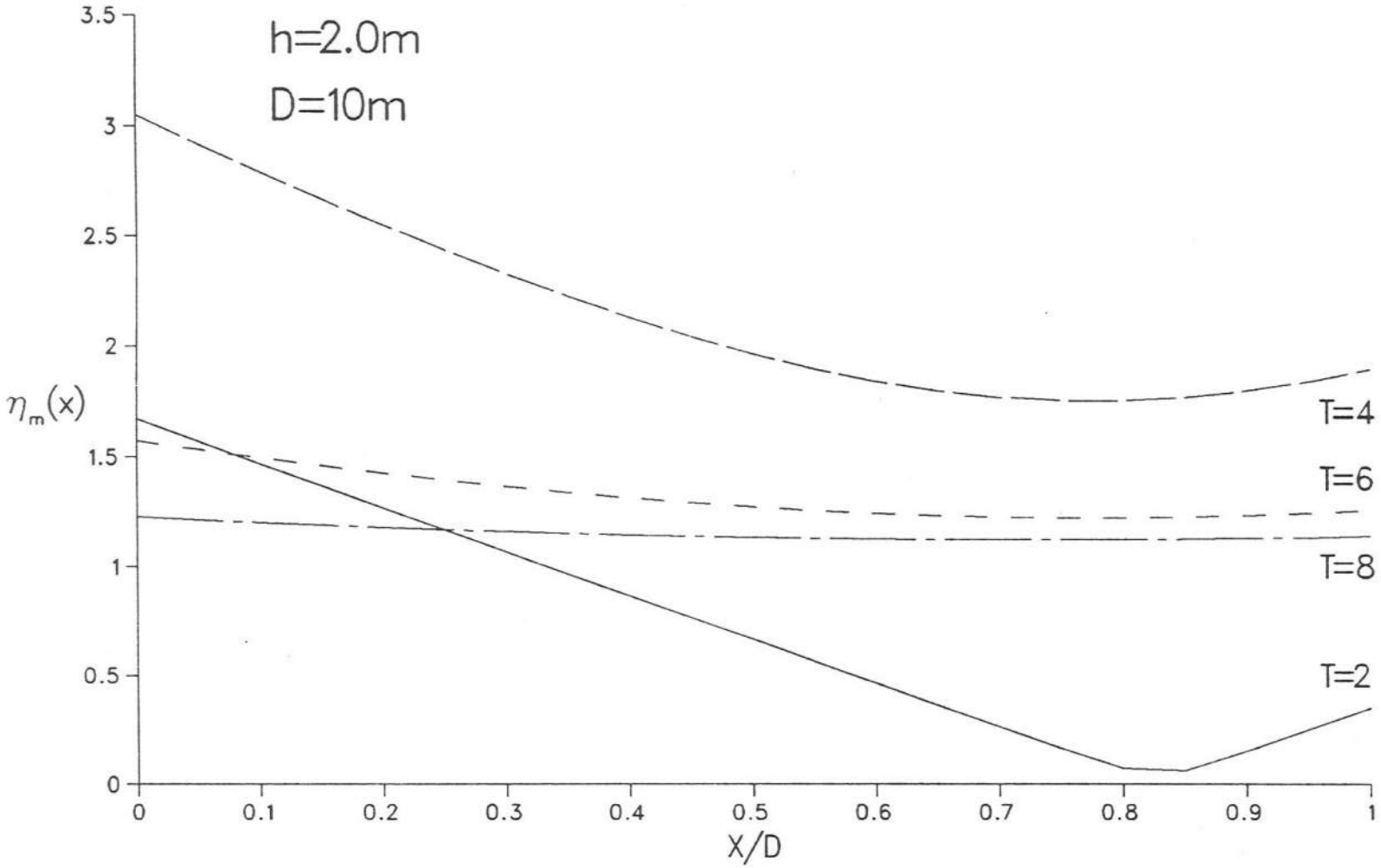

Fig. 21 - η_m as a Function of x/D with T = 2, 4, 6 and 8 sec for h = 2.0m and D = 10m.

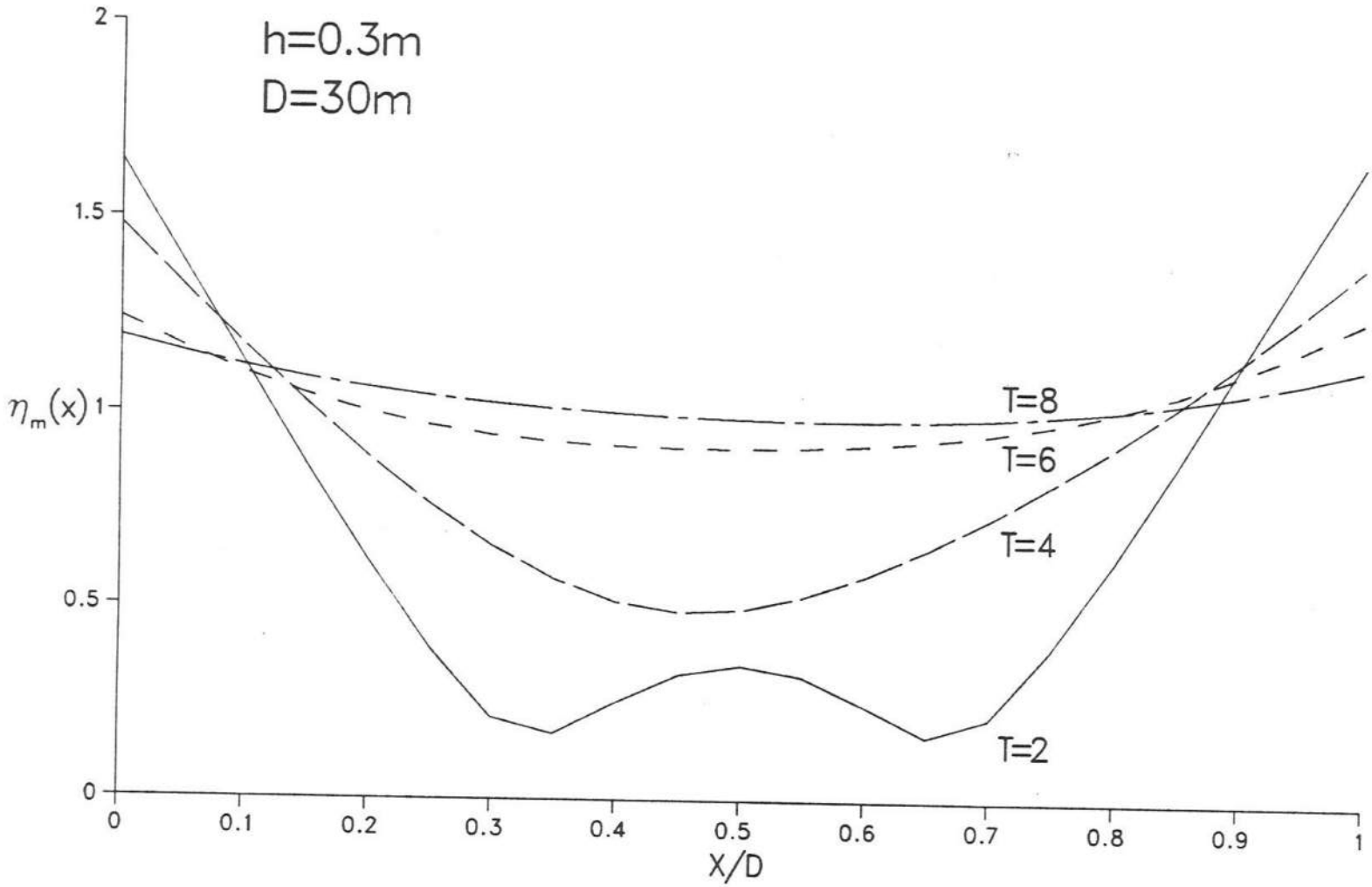

Fig. 22 - η_m as a Function of x/D with T = 2, 4, 6 and 8 sec for h = 0.3m and D = 30m.

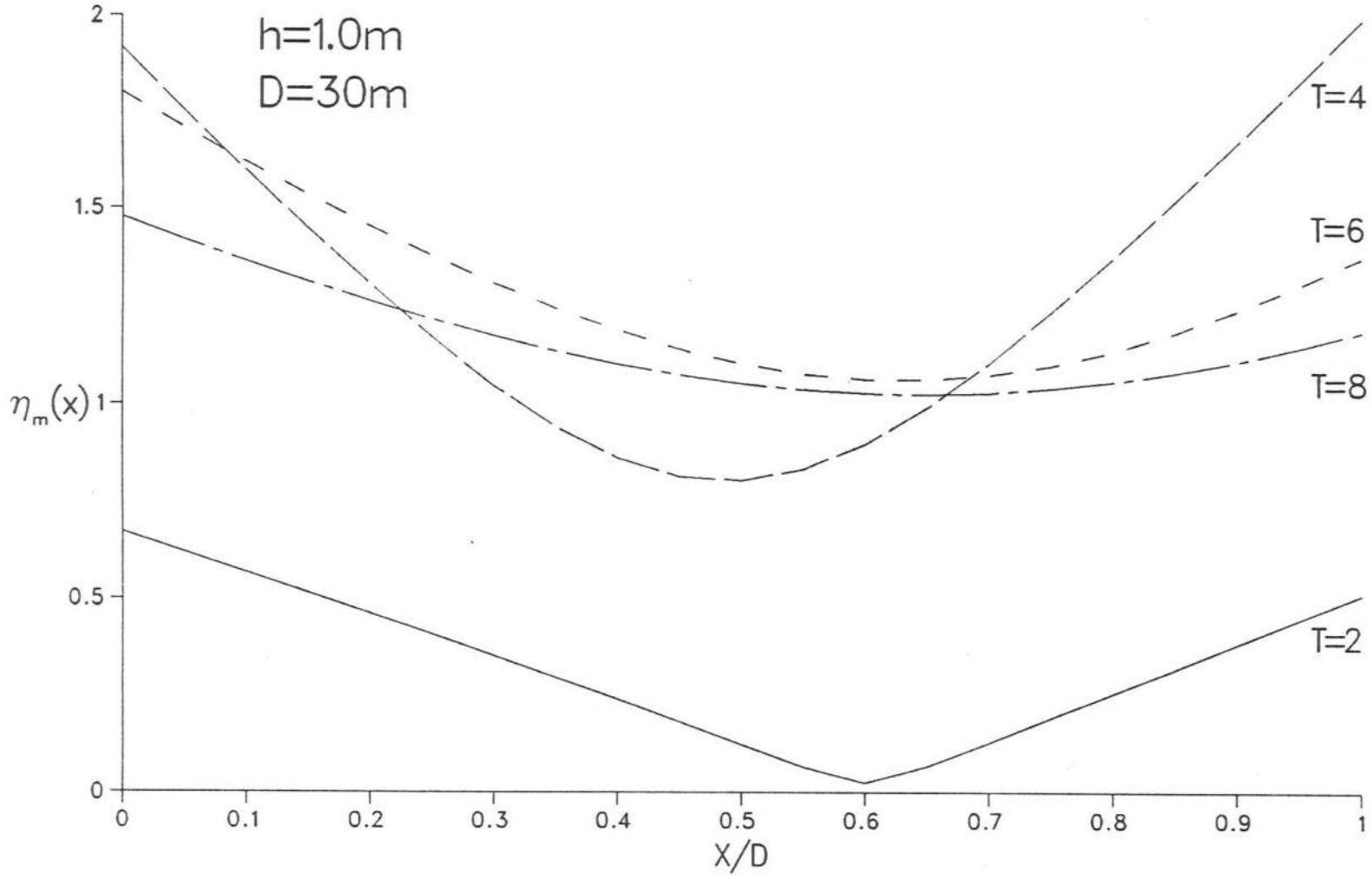

Fig. 23 - η_m as a Function of x/D with T = 2, 4, 6 and 8 sec for h = 1.0m and D = 30m.

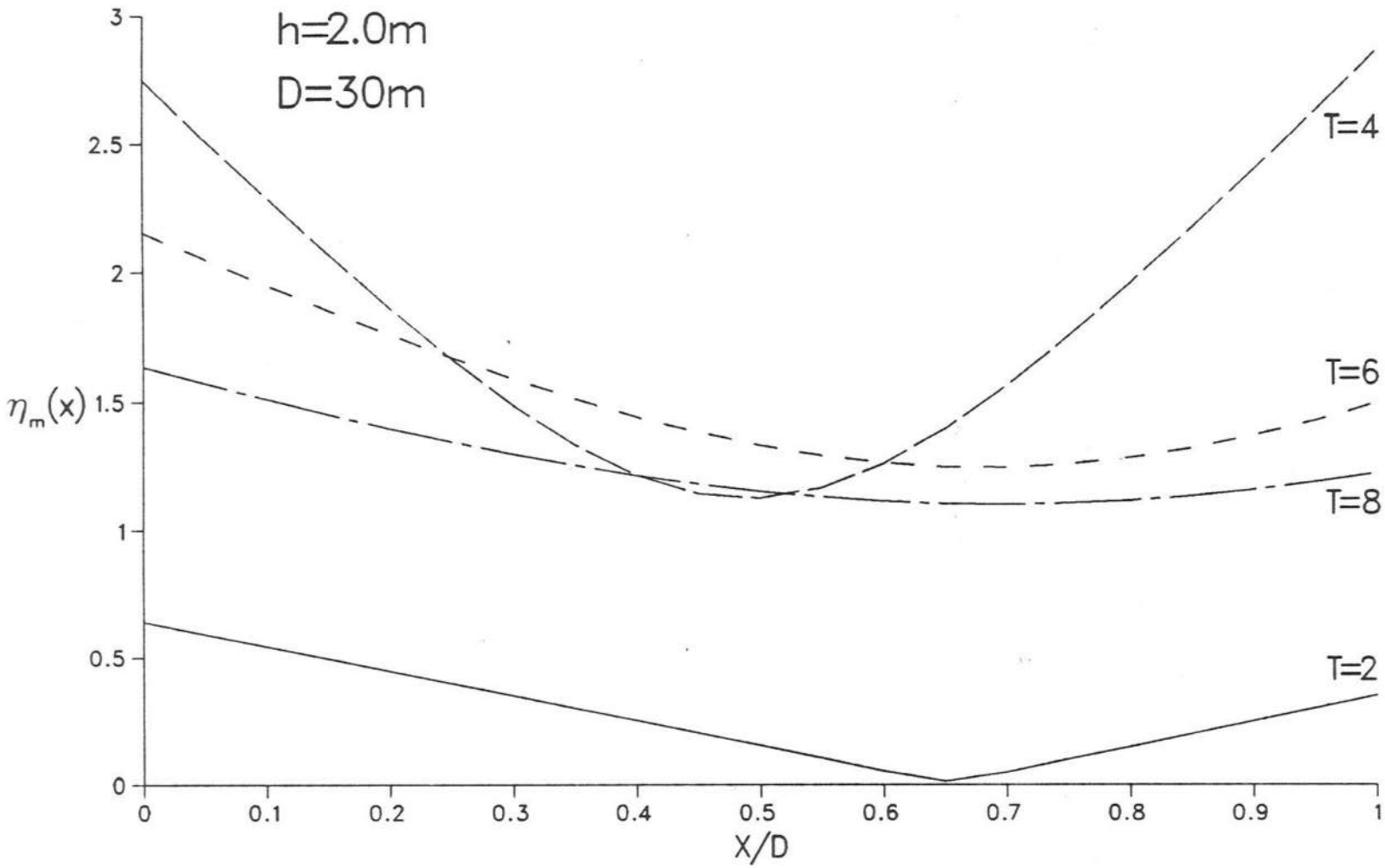

Fig. 24 - η_m as a function of x/D with T = 2, 4, 6 and 8 sec for h = 2.0m and D = 30m.

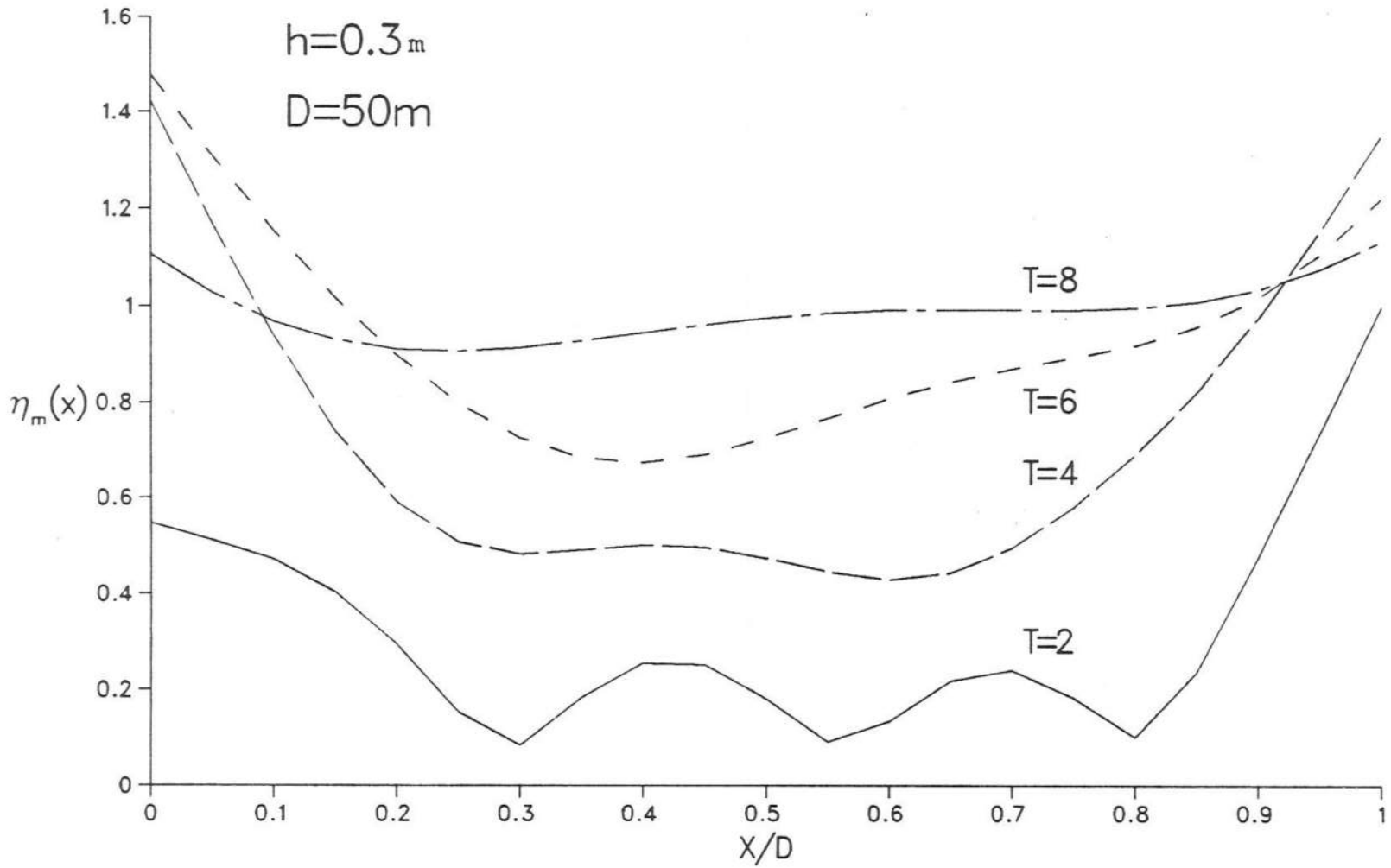

Fig. 25 - η_m as a Function of x/D with T = 2, 4, 6 and 8 sec for h = 0.3m and D = 50m.

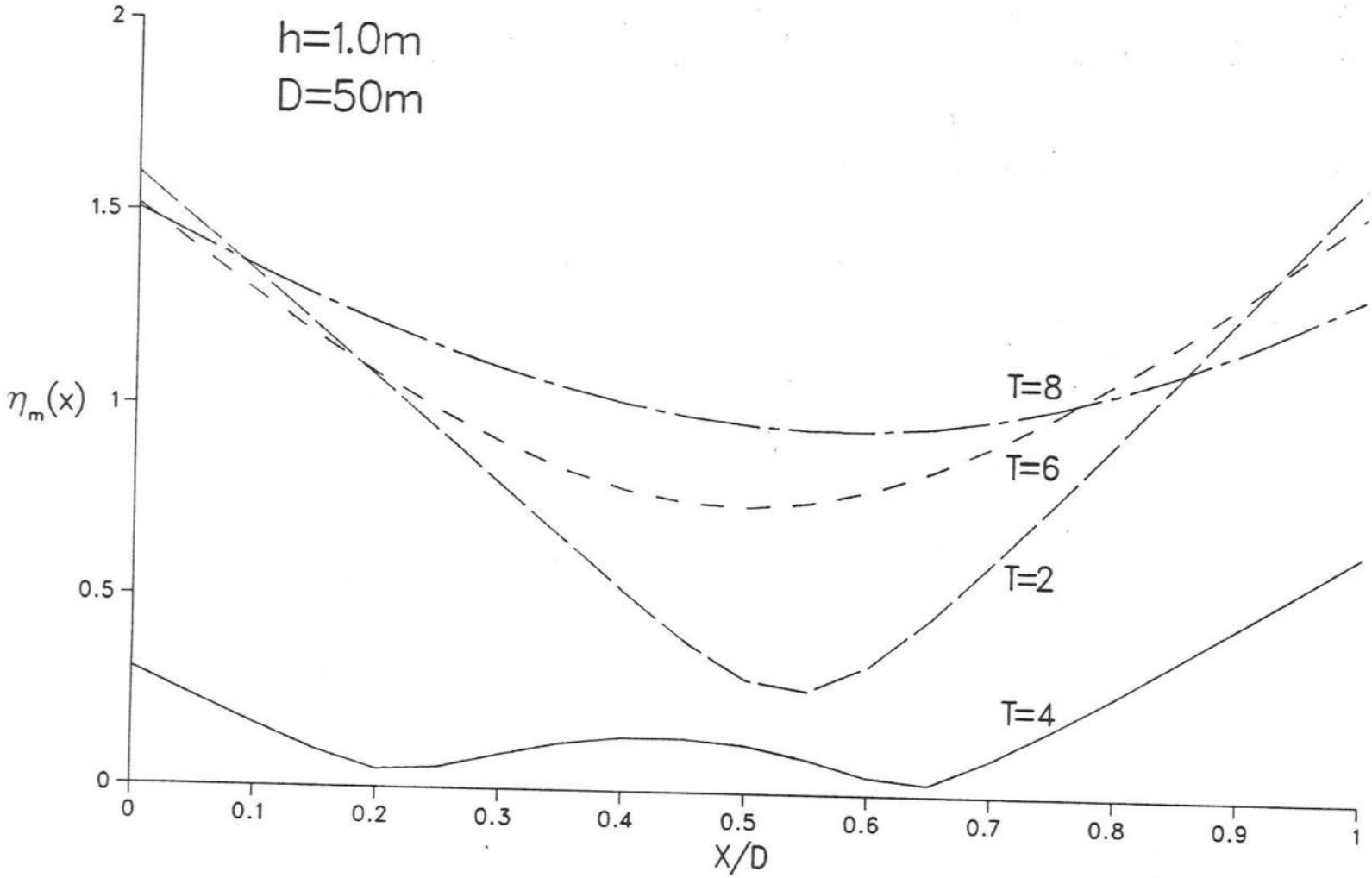

Fig. 26 - η_m as a Function of x/D with T = 2, 4, 6 and 8 sec for h = 1.0m and D = 50m.

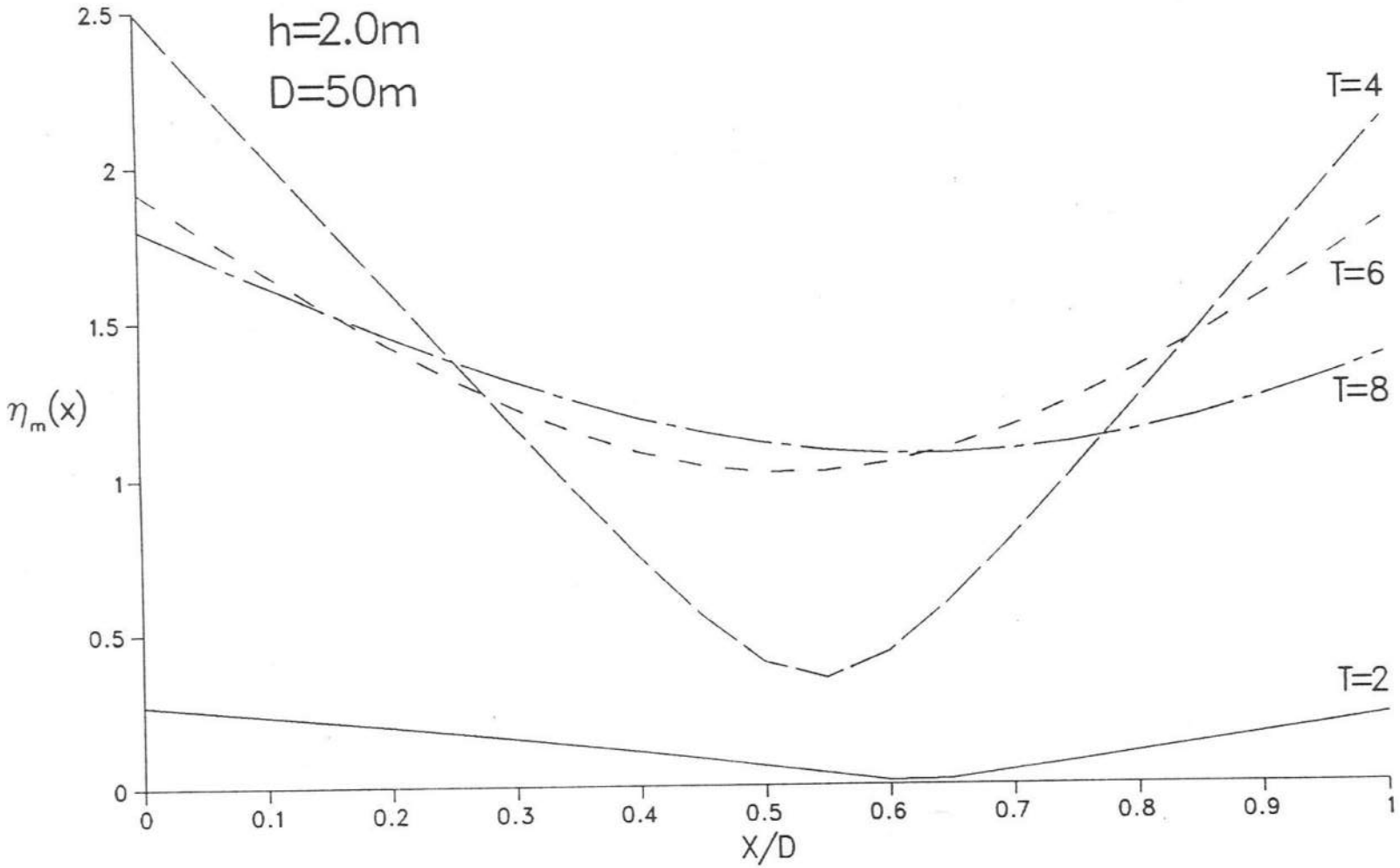

Fig. 27 - η_m as a Function of x/D with T = 2, 4, 6 and 8 sec for h = 2.0m and D = 50m.

4.2 Computed Results for Rigid Ice Floes

The computed results discussed in the following are based on the computation method for a vertically axisymmetric body given in Section 3.0. The ice floe of density ρ_i = 922.5 kg/m^3 is assumed to be cylindrical and floating freely in the sea water of density ρ = 1025 kg/m^3. The parameters E_i and ν are not needed for the rigid ice. The input parameters D and h are regarded as the diameter and height of the cylindrical ice floe. The water depth d needs to be specified as input for this case. The incident wave period T is varied to examine the effects of the size of the ice floe, D, relative to the incident wavelength, L. The additional input parameters required for the computation are the integer numbers N and M explained in Section 3.4. N = 30 and M = 8 are used in the following computation. Since some of the computed results were already presented by Kobayashi et al. (1986, 1987), the additional computation made for this report is limited to the case of D = 30 m, h = 1 m and d = 80 m corresponding to the rough first-year ice floe tracked during the Bering Air-Sea-Ice Study (BASICS) (Madsen et al., 1986; Kobayashi et al., 1987). The incident wave period is varied in the range T = 3 - 10 sec so that the computed results may be compared with those presented in Section 4.1. It should be noted that M=8 will not be sufficient for smaller values of T as explained in Section 3.4.

The computed oscillatory motions for the BASICS floe are presented in Fig. 28-30 where straight lines are drawn between the computed points for T = 3.0, 3.5, 4.0, ..., 10.0 sec. Figs. 28 and 29 show the surge amplitude $|\xi_1|$ and the heave amplitude $|\xi_2|$ normalized by the incident wave amplitude (H/2) as a function of the incident wave period T. Figs. 28 and 29 indicate that the cylindrical floe tends to behave like the fluid particle at the free

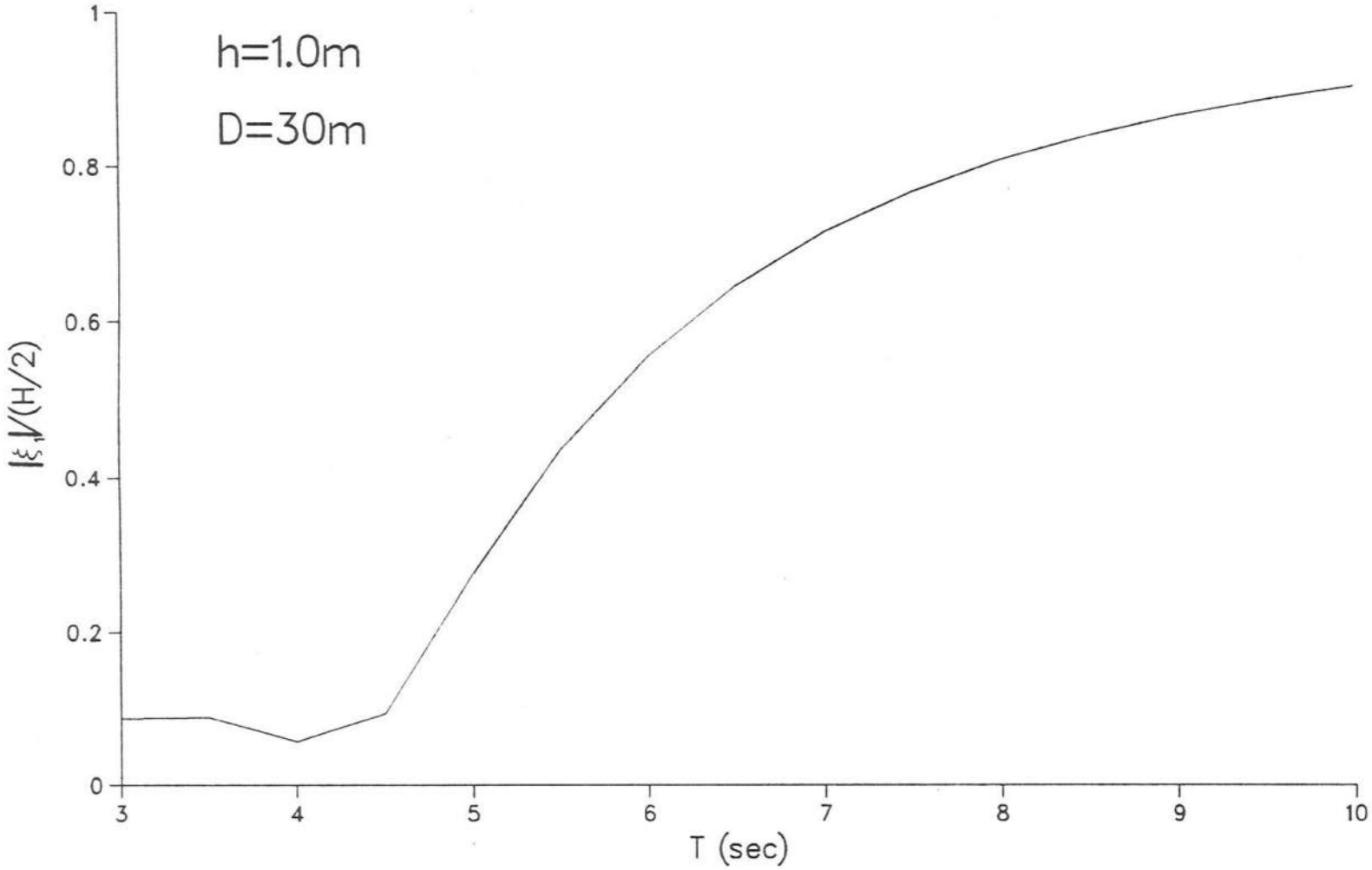

Fig. 28 - $|\xi_1|/(H/2)$ as a Function of T for h = 1.0m and D = 30m.

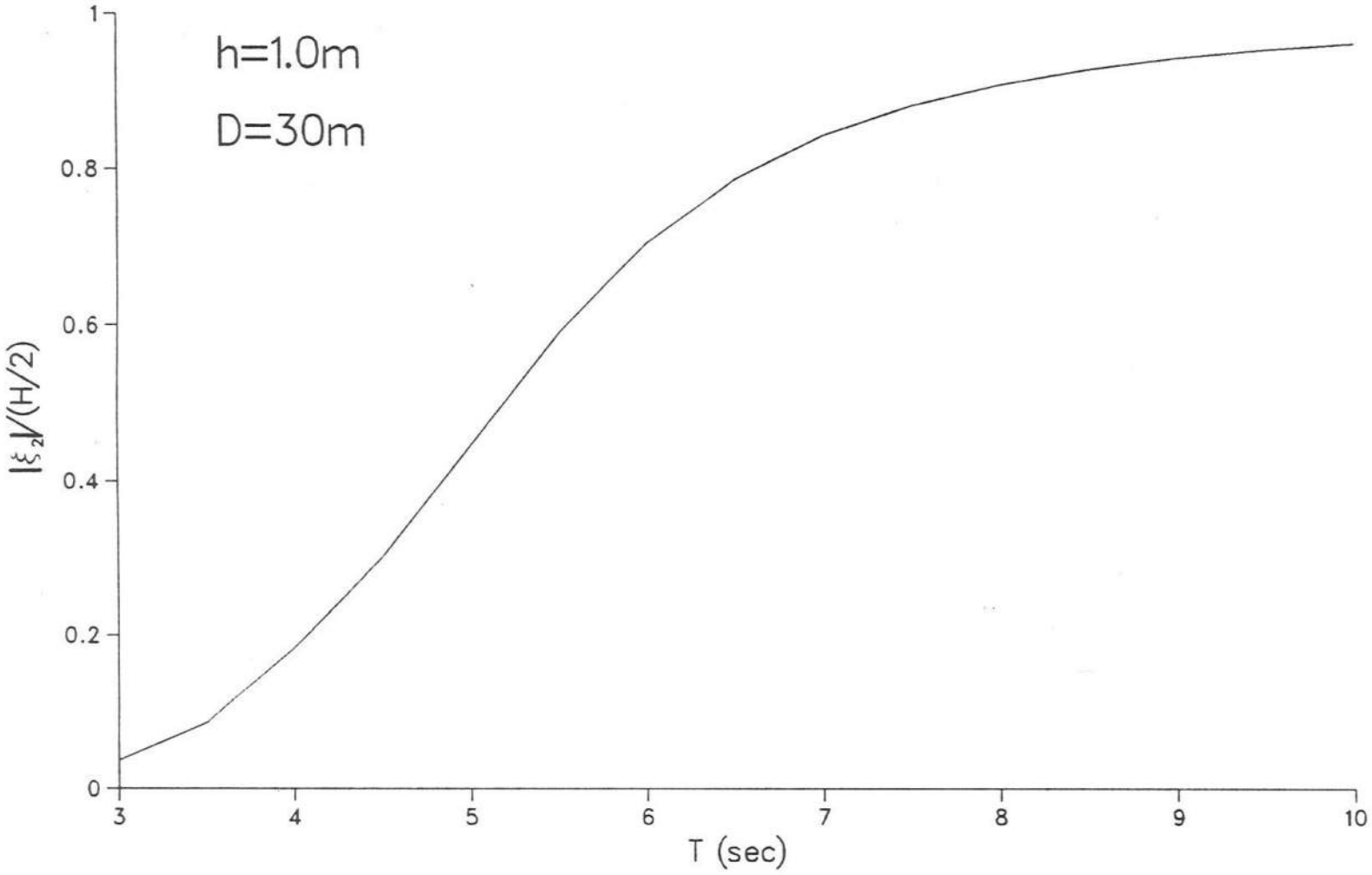

Fig. 29 - $|\xi_2|/(H/2)$ as a Function of T for h = 1.0m and D = 30m.

surface as T is increased for given D, that is, as the value of L/D becomes large. This finding is similar to that based on the small-scale model tests on small icebergs and bergy bits conducted by Lever et al. (1984). However, the heave amplitude for these models computed by Kobayashi et al. (1986) showed a sharp peak at the period of heave resonance, whereas the normalized heave amplitude shown in Fig. 29 for the BASICS floe does not have any sharp peak associated with the heave resonance. Using Eq. 99 and neglecting the effects of added mass and radiation damping, the period of the heave resonance for a cylindrical floe is approximately given by $T \simeq 2\pi(\rho_i h/\rho g)^{\frac{1}{2}}$ which is approximately 2 sec for the BASICS floe. This explains the lack of a sharp peak in Fig. 29. It should be noted that the heave resonance period increases with the ice thickness h and is larger for thick icebergs and bergy bits. On the other hand, Fig. 30 shows the computed pitch amplitude $|\xi_3|$ in radian divided by the incident wave amplitude (H/2) as a function of the incident wave period T. Fig. 30 indicates a broad peak at the period of approximately 5 sec.

The normalized wave drift force f_d defined by Eq. 109 is computed for the cylindrical BASICS floe and is shown in Fig. 31 as a function of the incident wave period T. The computed values of f_d decrease from $f_d \simeq 0.08$ at T = 3 sec and approaches zero rapidly as T is increased. The computed results shown in Fig. 31 are consistent with the computed results by Kobayashi et al. (1987) who plotted f_d as a function of L/D with L = wavelength in deep water. For the cylindrical ice floe $f_d \simeq 1/12$ as L/D approaches zero, whereas $f_d \simeq 1/8$ for the two-dimensional ice raft examined in Section 4.1. The difference between $f_d \simeq 1/12$ and 1/8 appears to be related to the fact that the two-dimensional analysis accounts for the scattered and radiated waves in the

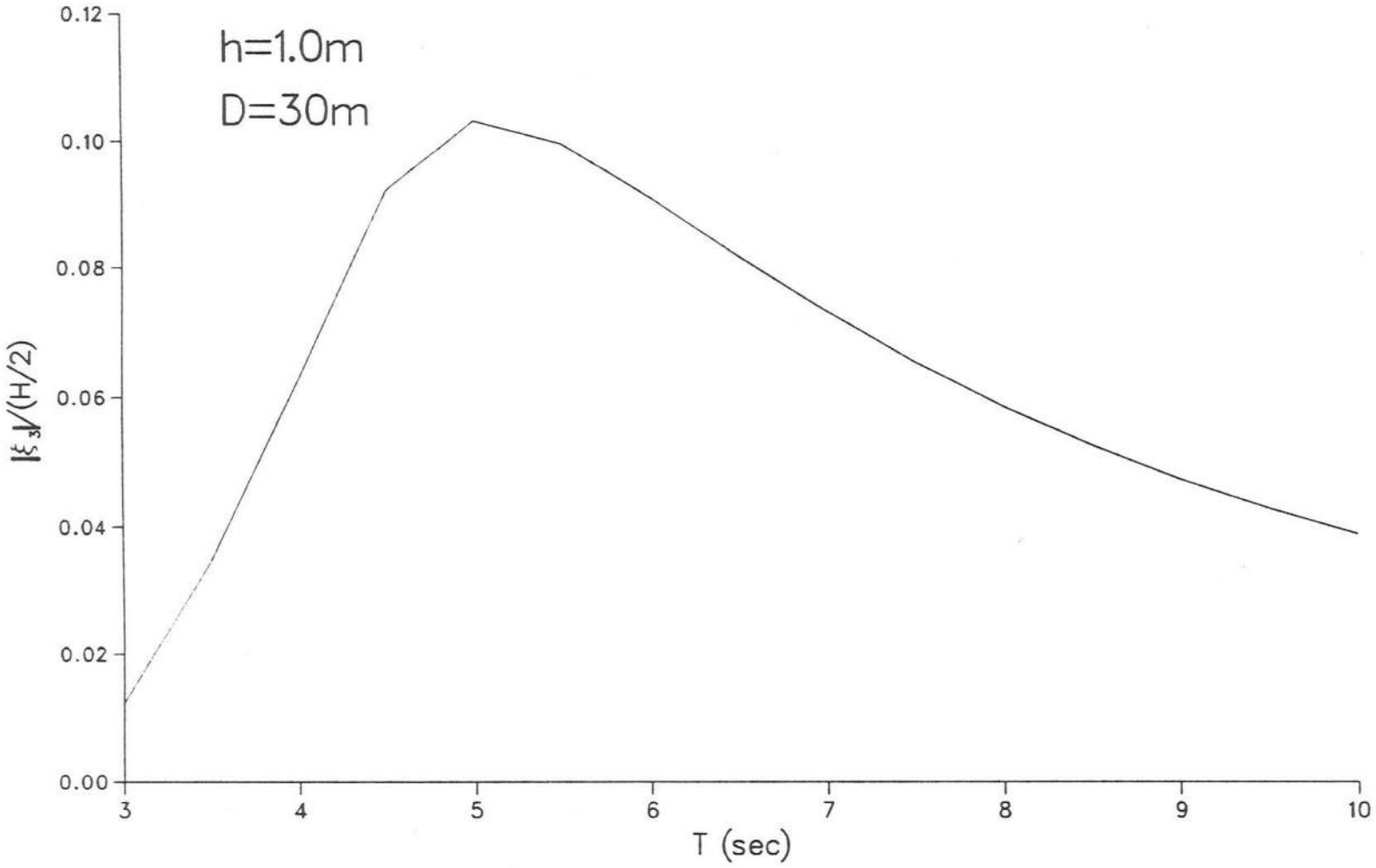

Fig. 30 - $|\xi_3|/(H/2)$ as a Function of T for h = 1.0m and D = 30m.

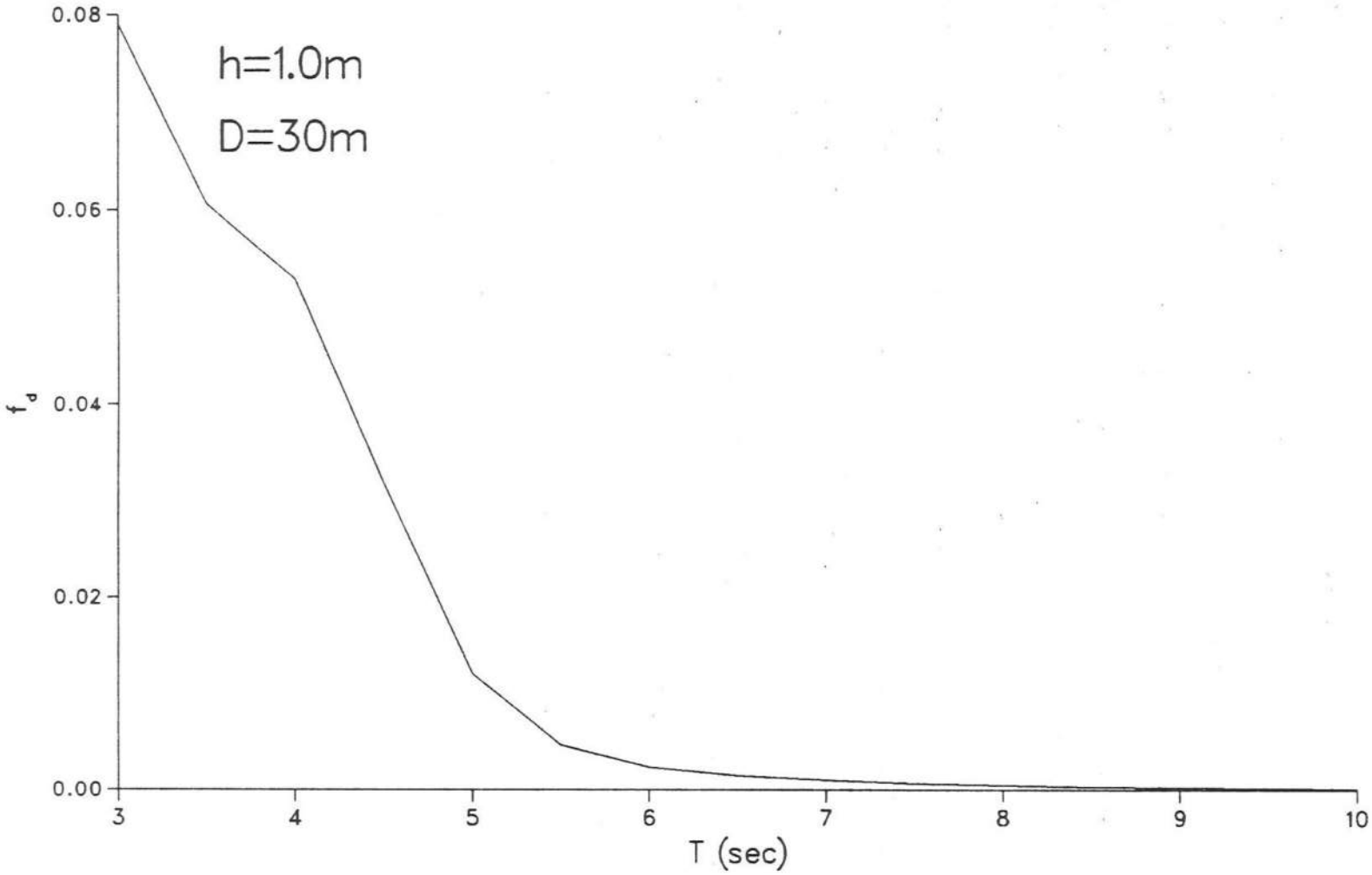

Fig. 31 - f_d as a Function of T for the Cylindrical Floe with h = 1.0m and D = 30m.

directions of $\theta = 0$ and π only. It should be noted that as the diameter D of the three-dimensional ice floe becomes large relative to the wavelength L, its oscillatory motion becomes negligible as has been the case with the two-dimensional ice raft examined in Section 4.1. Moreover, as the size D of the two-dimensional or three-dimensional floe becomes small relative to the wavelength L, the floe behaves like the fluid particle at the free surface. As a result, the behavior of the two-dimensional and three-dimensional floes are similar for the extreme cases. The trends of the variations of f_d with respect to T for the two-dimensional and three-dimensional cases shown in Section 4.1 and 4.2, respectively, are also similar.

The normalized wave drift force f_d discussed above accounts for the effects of the wave period T only for given ice floe characteristics. The dimensional wave drift force $F_d = (\rho g D H^2 f_d)$ from Eq. 109 is proportional to the square of the wave height H. Unfortunately, it is not possible to calculate the values of F_d on the ice floe since the associated values of H and T were not reported except that surface waves were observed to be negligible during BASICS (Madsen et al., 1986). Nevertheless, the assumption of negligible wave effects on the horizontal movement of the ice floe needs to be verified quantitatively by showing that the wave drift force was indeed negligible in comparison to the air-ice and ice-water drag forces which were found to be dominant (Madsen et al., 1986). The magnitude of the air-ice drag force on the cylindrical ice floe of diameter D may be expressed as (Madsen et al., 1986)

$$F_{ai} = \frac{\pi}{4} D^2 \rho_a C_{ai} |\vec{U}_{ai}|^2 \simeq \frac{\pi}{4} D^2 \rho_a C_{ai} U_a^2 \qquad (113)$$

in which ρ_a = air density ($\simeq 1.3$ kg/m^3), C_{ai} = air-ice drag coefficient, $\vec{U}_{ai}$ = reference wind velocity vector relative to the ice velocity vector and U_a =

reference wind speed. The assumption of $|\vec{U}_{ai}| \simeq U_a$ in Eq. 113 is normally appropriate (Wadhams, 1983). Madsen et al. (1986) estimated $C_{ai} \simeq 2.82 \times 10^{-3}$ for the BASICS floe where U_a was measured 3 m above the ice floe. As a result, the ratio of F_d to F_{ai} is given by

$$\frac{F_d}{F_{ai}} \simeq \frac{4 \rho g H^2 f_d}{\pi \rho_a C_{ai} D U_a^2} \tag{114}$$

The wave drift force may be neglected if the value of F_d/F_{ai} is much less than unity.

The wave conditions in the marginal ice zone may be very complicated since wind may generate waves in water openings (polynyas) inside the partial ice cover and swell may penetrate the partial ice cover from the open sea (Wadhams, 1983 & 1986). Furthermore, multiple scatterings and radiations will occur in the presence of multiple discrete ice floes. Consequently, it will be very difficult to predict the values of H and T to be used in Eq. 114. Limiting to the case of a single floe in the open water, use may be made of available deep-water wave prediction methods such as that given in the Shore Protection Manual (SPM) (U.S. Army Coastal Engineering Research Center, 1984). Assuming fetch-limited wind-generated waves, H and T may be predicted for given U_a and F where F = fetch length and U_a at the 3 m elevation needs to be adjusted following the SPM. H and T for computing F_d may be taken as the root-mean-square wave height and the spectral peak period, respectively. It should be noted that the wave drift force on a floating body in irregular waves contains the slowly varying component in addition to the computed mean component F_d (Løken et al., 1979; Pinkster et al., 1983). The slowly varying component is important for the design of mooring systems associated with large ships and floating offshore structures but may be neglected for predicting the net horizontal movement of an ice floe. The mean second- order force in a wave train consisting of a superposition of regular waves has been shown to be

the sum of the mean forces for each of the component waves (Pinkster et al., 1983).

Kobayashi et al. (1987) computed the values of F_d/F_{ai} for the BASICS floe as a function of U_a = 10 – 40 m/sec for F = 5 and 10 km. $C_{ai} = 2.82 \times 10^{-3}$ was used assuming that the presence of waves would not affect C_{ai}. It should be mentioned that the ice-water drag coefficient is more likely to be modified by the presence of the waves (Mollo-Christensen, 1986b). For the range U_a = 10 - 40 m/sec, H = 0.38 - 2.1 m and T = 2.6 - 4.6 sec for F = 5 km, while H = 0.54 - 3.0 m and T = 3.3 - 5.8 sec for F = 10 km. For the wave period smaller than 2.6 sec the value of M greater than 8 was found to be required to compute F_d accurately where Eqs. 110 and 111 were used to check the accuracy of the computation. The computed ratio of F_d/F_{ai} was much greater than unity and decreased as U_a was increased from 10 m/sec, although the fetch length F = 5-10 km might be very long for the partially ice-covered water. Kobayashi et al. (1987) hence concluded that the wave drift force should be evaluated more carefully even if surface waves might appear to be negligible visually.

5.0 SUMMARY AND CONCLUSIONS

5.1 Summary

The wave and ice interaction in partially ice-covered water has been investigated in this report. First, a brief review on previous studies on this subject has been given to identify various engineering and scientific problems which will require quantitative knowledge of the wave and ice interaction. The brief review has also indicated that the ice is presently modelled either as a thin elastic or inelastic plate or as a rigid body, depending on the nature of a specific problem, whereas linear wave theory is widely used to describe the wave motion. These basic assumptions regarding the ice and wave motion enable one to make use of the mathematical and numerical methods developed in other fields, although the wave and ice interaction in actual field conditions may be more complicated than the simplified interactions assumed in this report.

Second, the problem of the flexural response of elastic ice floes under the action of normally-incident regular waves in finite water depth has been formulated assuming that a row of the ice floes may be regarded as a long thin elastic raft of finite width in order to simplify the problem as a two-dimensional problem. The general solution obtained for the formulated two-dimensional problem has been shown to satisfy the matching conditions required at the edges of the ice raft unlike the approximate solution for deep water depth presented by Wadhams (1983, 1986). The formulated problem shows that the flexural response of the ice raft is related to the wave reflection and transmission coefficients which also affect the mean wave drift force acting on the ice raft. In order to reduce the required computational efforts, the general solution obtained for finite water depth has been approximated for deep water depth. The computational procedure for the approximate deep-water solution has then been explained in detail since the required algebraic

manipulations are not trivial.

Third, the oscillatory motion of a three-dimensional ice floe under the action of incident linear waves has been analyzed assuming that the ice floe is rigid and vertically axisymmetric. This analysis neglects the flexural motion of the ice floe but accounts for the surge, heave and pitch motions of the three-dimensional ice floe of finite thickness. The linear waves scattered and radiated by the oscillating ice floe have been computed using the boundary integral equation method developed for floating offshore structures. The mean wave drift force acting on the ice floe has been computed from the computed scattered and radiated waves in the far field. The adopted computation method has then been evaluated in terms of its accuracy and limitation by comparing available analytical and numerical solutions. the computation method has been found to be accurate within the limitation of the linearity assumption, although a better computation method is needed for a very large body relative to the incident wavelength for which a large number of harmonics are required to describe the circumferential variations of the wave motion.

Fourth, example computations have been made for elastic and rigid ice floes in deep water. For the two-dimensional elastic ice floe, computation has been made of the wave reflection and transmission coefficients, the normalized wave drift force and the normalized amplitude of the vertical flexural displacement of the ice. For the three-dimensional rigid ice floe, the normalized surge, heave and pitch amplitudes as well as the normalized wave drift force have been computed in the same was as was computed by Kobayashi et al. (1986,1987). Similarity and differences between the two-dimensional and three-dimensional results have been discussed. The qualitative behaviors of the two-dimensional and three-dimensional floes have been found to be similar for the extreme cases $D \ll L$ and $D \gg L$ in which D =

horizontal length of the floe and L = wavelength in deep water. The normalized wave drift forces computed by the two different methods have been found to be the same order of magnitude and vary with respect to wave period in a similar manner, although one method deals with a single rigid floe while the other assumes a row of identical elastic floes. Moreover, the computed results for the BASICS floe suggest that the wave drift force could be important and needs to be quantified even if surface waves appear to be negligible visually.

5.2 Conclusions

The analyses presented in this report are fairly idealized and need to be improved although these analyses elucidate the mechanism of the wave and ice interaction. It is desirable to develop a mathematical model which accounts for both flexural and oscillatory motions of an ice floe of arbitrary geometry. Moreover, the incident waves have been assumed to be linear, monochromatic and uni-directional in this report although directional random waves and swell as well as winds and currents are usually present even in the open water without ice floes. The presence of multiple floes and a structure in the partially ice-cover water will add the waves scattered and radiated multiply to the incident directional random waves and swell. Furthermore, the multiple ice floes may collide with one another or with the structure. The ice floes may also break under the wave action or due to the collision. Consequently, the actual wave and ice interaction in the partially ice-covered water is extremely complicated and difficult to describe mathematically. Field and laboratory data are hence essential for improving our capabilities of predicting the wave and ice interaction quantitatively.

APPENDIX I. - REFERENCES

Abramowitz, M. and Stegun, I. R. (1972). Handbook of Mathematical Functions, Dover, New York, N.Y.

Anderson, P. F. and Allyn, N. F. B. (1984). "Ice Management for Beaufort Sea Production Harbours," Proc. of 7th Symposium on Ice, IAHR, Hamburg, pp. 303-314.

Eatock Taylor, R. and Dolla, J. P. (1978). "Hydrodynamic Loads on Vertical Bodies of Revolution," Report No. OEG/78/6, Department of Mechanical Engineering, University College London, London, U.K.

Fenton, J. D. (1978). "Wave Forces on Vertical Bodies of Revolution," Journal of Fluid Mechanics, Vol. 85, pp. 241-255.

Frankenstein, S. (1986). "Interaction of Regular Waves with a Single Ice Floe," presented to the University of Delaware at Newark, Delaware, in partial fulfillment of the requirements for the degree of Master of Applied Science.

Goodman, D. J., Wadhams, P. and Squire, V. A. (1980). "The Flexural Response of a Tabular Ice Island to Ocean Swell," Annals of Glaciology, Vol. 1, pp. 23-27.

Harms, V. W. (1986). "Ice-Floe Wave Drift Experiments," Proc. of 18th Offshore Technology Conference, Vol. 1, Houston, Texas, pp. 9-15.

Isaacson, M. de St. Q. (1982). "Fixed and Floating Axisymmetric Structures in Waves," Journal of Waterway, Port, Coastal and Ocean Division, ASCE, Vol. 108, No. WW2, pp. 180-199.

Isaacson, M. de St. Q. and Dello Stritto, F. J. (1986). "Motion of an Ice Mass Near a Large Offshore Structure," Proc. of 18th Offshore Technology Conference, Vol. 1, Houston, Texas, pp. 21-23.

Johnson, R. C. and Nevel, D. E. (1985). "Ice Impact Structural Design Loads," Proc. of 8th International Conference on Port and Ocean Engineering Under Arctic Condition, Greenland, pp. 569-578.

Kagemoto, H. and Yue, D. K. (1986). "Interactions Among Multiple Three-Dimensional Bodies in Water Waves: An Exact Algebraic Method," Journal of Fluid Mechanics, Vol. 166, pp. 189-209.

Kheisin, D. Y. (1967). Dynamics of the Ice Cover. Technical Translation FSTC-HT-23-485-69, Defense Documentation Center, Cameron Station, Alexandria, Virginia.

Kobayashi, N. and Frankenstein, S. (1986). "Interaction of Waves with Ice Floes," Proc. of 8th Symposium on Ice, IAHR, Iowa City, Vol. 1, pp. 101-112.

Kobayashi, N. and Frankenstein, S. (1987). "Wave Drift Force on Ice Floe," Journal of Waterway, Port, Coastal and Ocean Engineering, Vol. 113, No. 5, pp. 476-492.

Kokkinowrachos, K., Bardis, L. and Mavrakos, S. (1983). "Drift Forces on One- and Two-Body Structures in Regular Waves," Proc. of 3rd International Conference on Behavior of Offshore Structures, Vol. 1, Hemisphere, New York, N.Y., pp. 467-489.

Lever, J. H., Reimer, E. and Diemand, D. (1984). "A Model Study of the Wave-Induced Motion of Small Icebergs and Bergy Bits." Proc. of 3rd Symposium of Offshore Mechanics and Arctic Engineering, New Orleans, La., pp. 282-290.

Longuet-Higgins, M. S. (1977). "The Mean Forces Exerted by Waves on Floating or Submerged Bodies with Applications to Sand Bars and Wave Power Mechanics," Proc. of Royal Society, London, U.K., Series A, Vol. 352, pp. 463-480.

Løken, A. E. and Olsen, O. A. (1979). "The Influence of Slowly Varying Wave Forces on Mooring Systems," Proc. of 11th Offshore Technology Conference, Houston, Texas, pp. 2325-2331.

Madsen, O. S. and Bruno, M. S. (1986). "A Methodology for the Determination of Drag Coefficients for Ice Floes," Proc. of 5th Symposium on Offshore Mechanics and Arctic Engineering, Tokyo, Japan, 1986.

Maruo, H. (1960). "The Drift of a Body Floating on Waves," Journal of Ship Research, Vol. 4, pp. 1-10.

Mei, C. C. (1983). The Applied Dynamics of Ocean Surface Waves. Wiley-Interscience, New York, N.Y.

Mollo-Christensen, E. (1983a). "Edge Waves as a Cause of Ice Rideup Onshore," Journal of Geophysical Research, Vol. 88, No. C5, pp. 2967-2970.

Mollo-Christensen, E. (1983b). "Interaction Between Waves and Mean Drift in an Ice Pack," Journal of Geophysical Research, Vol. 88, No. C5, pp. 2971-2972.

Newman, J. N. (1967). "The Drift Force and Moment on Ships in Waves," Journal of Ship Research, Vol. 11, pp. 51-60.

Pinkster, J. A. and Huijsmans, R. H. M. (1983). "The Low Frequency Motions of a Semi-Submersible in Waves," Proc of 3rd International Conference on Behavior of Offshore Structures, Vol. 1, Hemisphere, New York, N.Y., pp. 447-466.

Salvalaggio, M. A. and Rojansky, J. (1986). "The Importance of Wave-Driven Icebergs Impacting on Offshore Structure," Proc. of 18th Offshore Technology Conference, Vol. 1, Houston, Texas, pp. 29-34.

Sarpkaya, T. and Isaacson, M. de St. Q. (1981). Mechanics of Wave Forces on Offshore Structures. Van Nostrand Reinhold, New York, N.Y.

Sodhi, D. S. and El-Tahan, M. (1980). "Prediction of an Iceberg Drift Trajectory During a Storm," Annals of Glaciology, Vol. 1, pp. 77-82.

Squire, V. A. (1983a). "Numerical Modelling of Realistic Ice Floes in Ocean Waves," Annals of Glaciology, Vol. 4, pp. 277-282.

Squire, V. A. (1983b). "Dynamics of Ice Floes in Sea Waves," Journal of the Society of Underwater Technology, Vol. 9, No. 1, pp. 20-26.

Squire, V. A. (1984a). "On the Critical Angle of Ocean Waves Entering Shore Fast Ice," Cold Regions Science and Technology, Vol. 10, pp. 59-68.

Squire, V. A. (1984b). "A Theoretical, Laboratory, and Field Study of Ice-Coupled Waves," Journal of Geophysical Research, Vol. 89, No. C5, pp. 8069-8079.

U. S. Army Coastal Engineering Research Center (1984). Shore Protection Manual, Vol. 1, U. S. Government Printing Office, Washington, D.C.

Wadhams, P. (1973). "Attenuation of Swell by Sea Ice," Journal of Geophysical Research, Vol. 78, No. 18, pp. 3552-3563.

Wadhams, P. (1983). "A Mechanism for the Formation of Ice Edge Bands," Journal of Geophysical Research, Vol. 88, No. C5, pp. 2813-2818.

Wadhams, P., Squire, V. A. and Ewing, J. A. (1985). "Directional Wave Spectra Measured Near Ice Edges," Proc. of 8th International Conference on Port and Ocean Engineering Under Arctic Condition, Greenland, pp. 326-338.

Wadhams, P. (1986). "The Seasonal Ice Zone," The Geophysics of Sea Ice, ed. N. Untersteiner, Plenum, New York, N.Y.

APPENDIX II. - NOTATION

The following symbols were used in this report:

A = normalized wave amplitude in far field,

A_n = complex constants in Eq. 22,

a = added-mass coefficients,

a_n = complex constants in Eq. 26,

B = parameter defined by Eq. 106,

B_n = complex constants in Eq. 22,

b = radiation damping coefficients,

b_n = complex constants in Eq. 26,

C = hydrostatic stiffness coefficients; drag coefficients,

C_n = seven constants (n=1-7) introduced in Section 2.5,

D = horizontal length or diameter of ice floe,

D_i = flexural rigidity of ice,

d = water depth,

E = function defined by Eq. 102,

E_i = Young's modulus of ice,

F = force; fetch length,

f = normalized force,

G = Green's function,

g = gravitational acceleration,

H = wave height,

h = height or thickness of ice floe,

h_s = depth of submergence of ice floe,

i = $\sqrt{-1}$,

J = Bessel function of the first kind,

K_i = real positive number related to K_2 and K_3,

K_n = wave numbers determined from Eq. 23 or 24; from Eq. 55,

K_r = real positive number related to $K_2$and K_3,

k = incident wave number,

k_n = wave numbers determined from Eq. 27 or 28,

L = wavelength,

L_B = submerged body contour,

M = mass matrix coefficient; number of harmonics used for computation,

N = number of terms retained for computation; number of segments approximating L_B,

$\vec{n}_o$ = unit normal vector directed into body,

P_i = fluid pressure underneath ice raft,

R = wave reflection coefficient,

R_e = real part of complex variable,

r = radial coordinate,

S_B = submerged body surface,

T = incident wave period,

T_r = wave transmission coefficient,

t = time,

$\vec{U}$ = velocity,

u = variable defined in Eq. 75,

v = variable satisfying Eq. 82,

x = coordinate in direction of incident wave propagation,

Y = Bessel function of the second kind,

y = horizontal coordinate in right-handed Cartesian system,

z = vertical coordinate measured upwards from still water level,

z_i = vertical locations (i = 1,2,...I) at x=0 for matching solutions,

z_j = vertical locations (j=1,2,...,J) at x=D for matching solutions,

α = angle of $\vec{n}_o$ relative to horizontal plane,

β = $\pi D/L$,

ϵ = 1 or 1/2 depending on location of point $\vec{x}$,

ζ = vertical flexural displacement of ice raft; free surface displacement,

η = spatial variation of ζ,

η_m = normalized amplitude of ice displacement,

θ = polar coordinate with axis of $\theta = 0$ in x-direction,

ν = Poisson's ratio of ice,

ξ = complex amplitude of body motion,

ρ = density of sea water; density of air or ice,

σ = ω^2/g,

Φ = velocity potential,

ϕ = spatial variation of velocity potential, and

ω = wave angular frequency.

Subscripts

a = air,

d = mean wave drift force,

i = incident wave; ice,

j = mode of motion (j=1,2,3 and 4 corresponding to surge, heave, pitch and scattering, respectively),

n = component of exciting force (n=1,2 and 3 associated with surge, heave and pitch, respectively),

o = point on submerged body surface,

s - scattered wave,

1 - region $x \leq 0$ upwave of ice raft; surge motion,

2 - region $0 \leq x \leq D$ under ice raft; heave motion, and

3 - region $D \leq x$ downwave of ice raft; pitch motion.

Superscripts

m - harmonic of Fourier series, and

' - differentiation with respect to argument.